Eindhoven University of Technology

MASTER

Model order selection for robust-control-relevant identification

Tacx, P.J.M.M.

Award date:
2019

Link to publication

EINDHOVEN UNIVERSITY OF TECHNOLOGY

Department of Mechanical Engineering

Model Order Selection for Robust-Control-Relevant Identification

CST2019.087

Author:

P.J.M.M. Tacx *(0897675)*
P.J.M.M.Tacx@student.tue.nl

Supervisors:

dr. ir. T.A.E. Oomen
T.A.E.Oomen@tue.nl

ir. R. de Rozario
R.d.Rozario@tue.nl

Committee:

dr. A.Y. Pogromskiy
A.Y.Pogromskiy@tue.nl

dr. ir. G. Witvoet
G.Witvoet@tue.nl

dr. J.M.M.G. Noël
J.M.M.G.Noel@tue.nl

Eindhoven
17$^{\text{th}}$ December, 2019

Abstract

Next-generation motion systems are envisioned to be lightweight due to increasing demands regarding throughput and precision. As a result, flexible dynamic behaviour occurs within the control bandwidth. For this reason, conventional control strategies do no longer deliver the required performance. The aim of this research is to develop a joint system identification and robust control synthesis framework that is tailored towards next-generation motion stages. To synthesize robust controllers that achieve high performance, the identification step and the robust controller step are connected. In addition, the model should have a low order to enable a successful implementation of the resulting robust controller in a real-time environment. This is achieved by developing a model order selection rule which is based on a novel connection between the model order and the performance of the resulting controller. The developed framework is successfully applied to a simulation example showing that the proposed framework extends to existing methods.

Contents

List of abbreviations

Notation	Description
DOFs	Degrees of Freedom
FFR	Functional-model Floating Reticle
FRF	Frequency Response Function
GN	Gauss-Newton
LCF	Left Coprime Factorization
LFT	Linear Fractional Description
LMFD	Left Matrix Fraction Description
MFD	Matrix Fraction Description
MIMO	Multiple Input Multiple Output
p.c.c.	pseudo-canonical controllability
p.c.o.	pseudo-canonical observability
RCF	Right Coprime Factorization
RMFD	Right Matrix Fraction Description
SISO	Single Input Single Output
SK	Sanathanan and Koerner
SSV	Structured Singular Value

Chapter 1

Introduction

1.1   Technological Developments

In modern society, advancements in science and technology are a major driving factor in economic growth, welfare and quality of life [39, 41]. A key contributor to sustaining economic growth are advancements in the mechatronic industry [30, 57]. Examples include the semiconductor industry which enables exponential growth in computational power, thereby directly affecting science and daily life [40]. Also, developments in the electron microscopy enabling advancements from medical to material science [13]. Other applications include the printing industry and medical imaging [24, 20].

Many mechatronic systems contain a so-called motion stage that needs to be positioned with extreme accuracy during fast motions. Increasing demands regarding throughput have lead to a change in the design of next-generation motion stages. Observe that the velocity at which a motion stage moves highly influences the throughput. In general, the velocity is determined by Newton's second law,

$$F = ma. \tag{1.1}$$

Where F denotes the acceleration force, m denotes mass and a denotes the acceleration. To enhance the speed at which the stage moves, increasing the actuator force might be considered. However, the actuator force is often limited due to volumetric limitations or thermal constraints. Therefore, to enhance the throughput of next-generation motion systems, light-weight motion stages are indispensable.

1.2   High-Precision Motion Control

Motion stages typically need to be positioned with high accuracy during fast motions in six Degrees of Freedom (DOFs). To obtain motion stages that achieve the desired performance, feedback-control is indispensable. Traditionally, motion stages are approximated as a rigid body. Then, by an appropriate choice of the input and output decoupling matrices, an approximately diagonal system is obtained. Therefore, each output is only affected by one input. This allows the implementation of Single Input Single Output (SISO) controllers [60].

Next-generation motion stages are envisaged to be inherently light-weight. Therefore, resonances occur at a lower frequency. In addition, increasing demands regarding throughput and precision

leads to increasing demands regarding the closed-loop bandwidth. For these reasons, the flexible dynamic behaviour occurs within the control bandwidth. In general, the flexible dynamics are not aligned with the DOFs. Therefore, next-generation motion stages are inherently multivariable. Hence, SISO controllers can no longer achieve the desired performance.

For the design of a controller for next-generation motion stages, a model-based controller synthesis method should be adopted for two reasons. (i) Manually tuning an inherently multivariable controller is practically infeasible. (ii) A model is crucial to explore the limits of a system, i.e. tradeoff between robustness and performance.

1.3 Modelling High Precision Motion Systems

A model is an approximation of reality. Therefore, a model cannot encompass the complete behaviour a true system. Robust control takes modelling errors explicitly into account by considering a model set which encompasses the true system. The model set is constructed around a nominal model with a perturbation that reflects the model uncertainty. Regarding the construction of the model set, the following requirements are formulated.

(R1) The model set should enable the synthesis of a robust controller that achieves high performance.

(R2) The model set should enable the synthesis of a low-order controller for successful implementation in a real-time environment.

In view of (R2), a low-order nominal model is desired for two reasons. (i) For the synthesis and implementation in a real-time environment, a low-order controller is required. As the order of the robust controller is directly related to the order of the nominal model, synthesizing a low-order nominal model is necessary. (ii) Second, next-generation motion stages are equipped with many sensors and actuators, more than the number of DOFs, which increases model complexity significantly. From a numerical perspective, a high model complexity is undesirable. It is known that model complexity is directly related to model order. Therefore, to obtain a nominal model with limited complexity, selecting a low-order nominal model is necessary.

To address (R1), the model set has to be selected in view of the control goals. Therefore, joint system identification and robust controller synthesis method is necessary. To address (R1), the identification of the model set should be connected to the robust controller synthesis. In [7] and [60], a joint system identification and robust control synthesis approach is presented. However, the connection between the identification of the model set and robust controller synthesis appeared to be a performance-limiting factor. In [14, 51], a first step is taken in view of (R1). In this approach, the control objective is absorbed into the identification of the nominal model. However, the model structure used in the approach resulted in a conservative synthesis of the robust controller which hampers performance significantly. In [42, 47], the above approach is improved by considering a novel model structure, enabling the estimation of a nonconservative robust-control-relevant model set.

Next, observe that in view of (R1) an accurate nominal model is desired. In general, an accurate model is achieved by high-order models. This, in turn, leads to a high-order controller, thereby violating (R2). This motivates the investigation on how the order of the nominal model influences

the performance of the model set. Secondly, the tradeoff between (R1) and (R2) motivates an order selection procedure. Therefore, the following research objectives are formulated.

Research Objective 1. Investigate a connection between the performance of the model set and the order of the model set.

Research Objective 2. Develop an order selection procedure to break the tradeoff between the performance of the robust controller and the order of the nominal model.

For successful identification of the model set, the nominal model should be suitably parameterized. The parametrization should enable (R2), i.e., the parametrization should enable an order selection procedure. Secondly, for a selected order of the nominal model, the parametrization should describe a rich class of systems. Lastly, the parametrization should enable numerically reliable synthesis of the nominal model. Therefore, based on these findings, the following research objective is formulated.

Research Objective 3. Develop a parametrization for the nominal model, that enables (i) the selection of a low-order nominal model in view of (R2) and (ii) numerically reliable estimation of the nominal model.

1.4   Experimental Setup

Over the last decade, many theoretical contributions are developed regarding next-generation motion stages. However, in academic environments, the number of experimental setups representative for next-generation motion stages is limited. In the motion laboratory of the Eindhoven University of Technology, the Functional-model Floating Reticle (FFR) is available to experimentally validate these control algorithms.
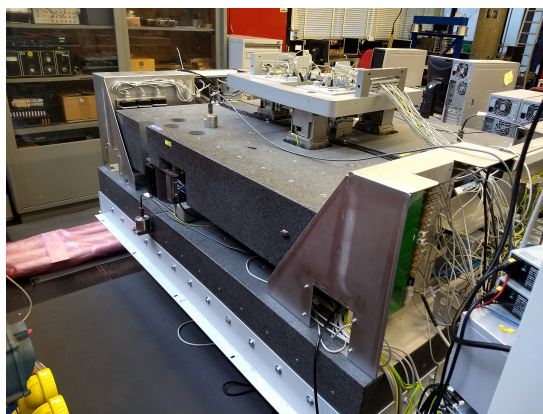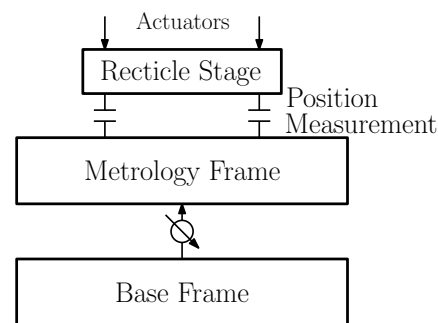
Figure 1.1 (a) Overview of the FFR setup. (b) Figure showing the reticle stage.

In Figure 1.1b, the FFR is schematically shown with its main components. The setup consists of two independently controlled systems. The first system is the active vibration isolation system. It consists of a base frame which is mounted to the floor. On top of the base frame, a metrology frame is mounted which is weakly suspended by air mounds. To enhance vibration isolation properties, the system is equipped with Lorentz actuators to actively suppress disturbances. For

more details on this part of the setup, see [9, 8]. The second system is the reticle stage. The position of the reticle stage is measured with respect to the metrology frame. The actuation is performed relative to the base frame. The reticle stage is considered to be a representative as next-generation motion stage as it contains a light-weight motion stage and it contains 14 actuators and 14 sensors. Therefore, the following research objective is formulated.

Research Objective 4. Bring the FFR in service, and experimentally validate the joint-identification-control framework on the FFR.

1.5 Thesis Outline

This thesis is ordered as follows. In Chapter 2, the robust control problem and the corresponding control-relevant-identification procedure is elucidated. Chapter 3, is considered to be the main contribution of this thesis. In this chapter, the robust-control-relevant model structure is developed, enabling a relation between the performance of the robust controller, the estimation of the nominal model, and the selection of the model order. The parametrization of the nominal model is derived in Chapter 4. A numerical method to reliably identify the robust-control-relevant model set is developed in Chapter 5. The robust controller synthesis including the control objectives is discussed in Chapter 6. The reticle stage is brought into service, by repairing broken hardware and writing suitable code. This process is elaborated in Appendix A. However, due to time limitations, the theoretical framework is not validated experimentally. Instead, a representative simulation example is provided in Chapter 7. In Chapter 8, the conclusions and recommendations are given.

Chapter 2

Robust Control and Robust-Control-Relevant System Identification

In this research, a robust-control-relevant identification framework is developed that enables the synthesis of robust controllers that achieve high performance and successful application in a real-time environment. To arrive at the robust-control-relevant identification procedure, first, the robust control framework is investigated. Thereafter, the robust-control-relevant identification approach is investigated. In the last section, the main contribution addressed in this research is formulated.

2.1 Robust Control

The aim of this section is to investigate the robust control strategy. Therefore, first, the control criterion is investigated. Second, the robust control problem is elaborated, which is a crucial step in the development of the joint identification and robust control framework.

2.1.1 Control Criterion

A key property of a robust controller is that it achieves optimal performance with respect to a control criterion. For this reason, the formulation of a suitable control criterion is crucial. To arrive at a suitable control criterion, consider the closed-loop block diagram in Figure 2.1a. Herein, $C \in \mathbb{C}^{n_u \times n_y}$ denotes the controller and $P_o(s) \in \mathbb{C}^{n_y \times n_u}$ denotes the true plant.
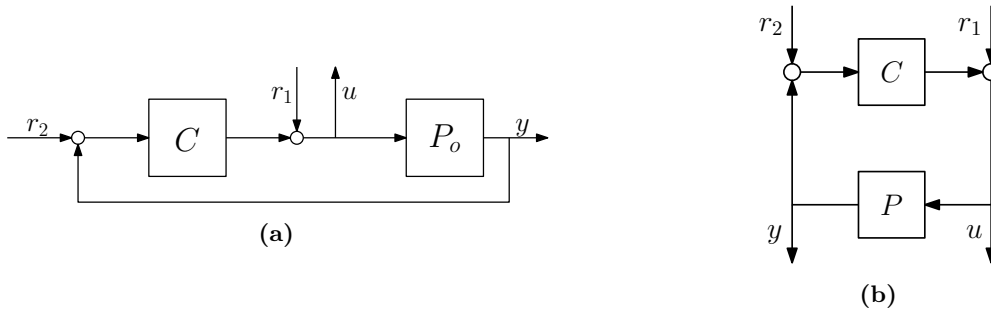
Figure 2.1 (a) Closed-loop of the true system P_o and the controller C. (b) Four-block feedback interconnection $T(P, C)$.

Next, consider the four-block-interconnection in Figure 2.1b. Herein, the closed-loop transfer function $T(P, C)$ is defined as,

$$T(P, C) = \begin{bmatrix} r_2 \\ r_1 \end{bmatrix} \mapsto \begin{bmatrix} y \\ u \end{bmatrix}, \quad \begin{bmatrix} P \\ I \end{bmatrix} (I + CP)^{-1} \begin{bmatrix} C & I \end{bmatrix} \tag{2.1}$$

Based on the four-block feedback interconnection, the performance criterion is formulated.

Definition 1. Performance Criterion. Given the four-block-interconnection system according to Eq. (2.1). Then, the performance criterion is defined as,

$$\mathcal{J}(P, C) = \|WT(P, C)V\|_\infty. \tag{2.2}$$

Where, $W = \text{diag}(W_y, W_u)$ and $V = \text{diag}(V_2, V_1)$ denote the output- and input-weighting filter.

The weighting filters may be used to specify the performance objectives. The value of $\mathcal{J}(P, C)$ gives an indicates how well the performance objectives are satisfied. A small value of the control criterion means high performance, whereas a large value means a poor performance.

The usage of four-block-interconnection, Eq. (2.1), in combination with the $\mathcal{H}_\infty$-norm is adopted, as it guarantees internal stability of the resulting closed-loop system [68]. Second, the selected performance criterion allows specifying the control objective in an intuitive manner using loop-shaping-based techniques [37].

Based on the performance criterion, Definition 1, the definition of the optimal controller is formulated,

$$C^{opt} = \arg\min_C \mathcal{J}(P_o, C). \tag{2.3}$$

However, the true system P_o is not explicitly known. Therefore, a mathematical description of the true system is required. This will be the topic of the next section.

2.1.2   Robust Control

Direct minimization of Eq. (2.3) is untractable as an exact mathematical description of the true system P_o is not explicitly known. Therefore, a nominal model $\hat{P}(n_x)$ of order n_x is constructed to approximate the behaviour of the true system P_o. Next, consider the definition of the nominal controller C^{NP},

$$C^{NP} = \arg\min_C \mathcal{J}(\hat{P}(n_x), C). \tag{2.4}$$

However, a mathematical model is always an approximation of reality. Therefore, the nominal model $\hat{P}(n_x)$ cannot capture the true behaviour of the true system P_o. Instead, a model set $\mathcal{P}(n_x)$ is constructed which encompasses the true system P_o,

$$P_o \in \mathcal{P}(n_x). \tag{2.5}$$

The model set is constructed around a nominal model $\hat{P}(n_x)$ of order n_x with a model uncertainty $\Delta_u \in \mathcal{RH}_\infty$. The nominal model and the model uncertainty are related to the model set through an upper Linear Fractional Description (LFT)-based structure,

$$\mathcal{P}(n_x) = \left\{ P | P = \mathcal{F}_u(\hat{H}(\hat{P}(n_x)), \Delta_u), \|\Delta_u\|_\infty \leq \gamma \right\}. \tag{2.6}$$

Where, γ denotes the size of the model uncertainty Δ_u. The upper LFT is defined as,

$$\mathcal{F}_u(\hat{H}, \Delta_u) = \hat{H}_{22} + \hat{H}_{21}\Delta_u(I - \hat{H}_{11}\Delta_u)^{-1}\hat{H}_{12}. \tag{2.7}$$

By definition, $\hat{H}_{22} = \hat{P}(n_x)$. To see this, consider $\gamma = 0$, as a result $\Delta_u = 0 \implies \mathcal{F}_u(\hat{H}, 0) = \hat{P}(n_x)$. Furthermore, $\hat{H}_{12}$, $\hat{H}_{21}$ and $\hat{H}_{11}$ depend on the selected model structure.

Next, observe that the performance criterion specified in Definition 1, may be evaluated for all candidate systems in $\mathcal{P}(n_x)$. This leads to the formulation of the worst-case performance,

$$\mathcal{J}_{WC}(\mathcal{P}(n_x), C) = \sup_{P \in \mathcal{P}(n_x)} \mathcal{J}(P, C). \tag{2.8}$$

Based on the formulation of the worst-case performance, Eq. (2.8), a performance guarantee is formulated for a controller C,

$$\mathcal{J}(P_o, C) \leq \mathcal{J}_{WC}(\mathcal{P}(n_x), C) \tag{2.9}$$

This means that if a controller achieves a certain worst-case performance, the controller achieves at least the same performance when applied to the true system. Therefore, the bound in Eq. (2.9) may be used for the synthesis of the robust controller,

$$C^{RP} = \arg\min_C \mathcal{J}_{WC}(\mathcal{P}(n_x), C). \tag{2.10}$$

Observe that for the robust controller, Eq. (2.10), a performance and stability guarantee is provided. However, for the controller that achieves nominal performance, Eq. (2.4), neither a stability guarantee nor a performance guarantee can be given when applied to the true system. This is the key motivation for considering a robust control strategy.

2.2 Robust-Control-Relevant Model Set Estimation

Note that the worst-case performance bound, Eq. (2.9), depends on the model set $\mathcal{P}(n_x)$. Therefore, the performance achieved by the robust controller C^{RP} depends on the quality of the model set. To see this, consider a large model set $\mathcal{P}(n_x)$. As a large model set is considered, the model set encompasses the true system, hence, Eq. (2.5) is satisfied. However, the robust controller, Eq. (2.10), needs to be robust the entire model set. Consequently, the performance achieved by the robust controller is low.

To enable the synthesis of a robust controller that achieves high performance, the model set should be small. Therefore, the control objectives are incorporated within the identification procedure of the model set. This is achieved by considering a similar expression as in Eq. (2.10),

$$\mathcal{P}^{RCR}(n_x) = \arg\min_{\mathcal{P}(n_x)} \mathcal{J}_{WC}(\mathcal{P}(n_x), C), \text{ s.t. } P_o \in \mathcal{P}(n_x). \tag{2.11}$$

Note that Eq. (2.11) depends on the controller C. However, during the identification step, C^{RP}, is not yet available. To enable a tractable identification procedure, a stabilizing experimental controller, C^{exp}, is implemented. In general, the experimental controller C^{exp} is not optimal. Consequently, if the distance between C^{exp} and C^{RP} is large, iterative robust-control-relevant identification and robust controller synthesis may be advantageous [3, 11, 14, 46]. The identification of the model set is formally defined in the following definition.

Definition 2. Robust-control-relevant model set. The robust-control-relevant model set with the experimental controller C^{exp} is defined as,

$$\mathcal{P}^{RCR}(n_x) = \arg \min_{\mathcal{P}(n_x)} \mathcal{J}_{WC}(\mathcal{P}(n_x), C_{exp}), \text{ s.t. } P_o \in \mathcal{P}(n_x). \tag{2.12}$$

2.2.1 Robust-Control-Relevant Model Order Selection

For successful application in a real-time environment, it is important that the order of the robust controller is low. Observe that the order of the robust controller is directly related to the order of the weighting filters, the synthesis method and the order of the nominal model n_x [68, 54]. This motivates the selection of a low-order nominal model for two reasons. (i) Typically, the synthesis method is fixed. Furthermore, the order of the weighting filters is typically low and, compromising on the control objectives specified in the weighting filter is not preferable. (ii) Second, a low-order nominal model is also desired from a numerical point of view, as model complexity is related to the order of the nominal model. Therefore, for successful numerical estimation, it is desirable to estimate a low-order nominal model.

The order selection process of the nominal model leads to a tradeoff. To see this, consider a high order nominal model $\hat{P}_h$. As a consequence, $\hat{P}_h$ contains most of the behaviour of the true model P_o. Therefore, the corresponding model set $\mathcal{P}_h$ is small. This means that the controller needs to be robust for a small model set. Hence, the performance of the robust controller is high. However, as the order of the nominal model is high, the order of the robust controller is also high.

Analogously, a low order nominal model leads to a low order robust controller with a poor performance. To break the tradeoff, the order of the nominal model, n_x, should be penalized during the identification process of the robust-control-relevant model set, Definition 2.

In [61], model order selection is studied from the perspective of the robust-control-relevant identification framework. However, no specific model order selection rule is given. Model order selection for the nominal model that constitutes a model set using $\mathcal{H}_\infty$ bounded perturbations has been studied in the set-membership framework [22, 38]. However the framework is considered to be unsuitable for three reasons. First of all, an additive uncertainty is considered instead of a dual-Youla-Kučera as considered in this research. Second, the proposed approach requires the true system to be explicitly known. Third, the proposed algorithm suffers from a large computational complexity, which inflates especially for next-generation motion stages which contain many inputs and outputs and use large sample frequencies.

Model order selection is largely studied in the prediction error framework, see [56, 26] and references therein. Essentially, these methods penalize for the addition of model order by adding a so-called regularization term. In this research, the concept of adding a regularization term

is adopted, therefore, using Eq. (2.12) the following definition of the optimal model order is considered,

$$n_x^* = \arg\min_{n_x} \mathcal{J}_{WC}(\mathcal{P}(n_x), C_{exp}) + f(n_x), \text{ s.t. } P_o \in \mathcal{P}. \tag{2.13}$$

Where $f(n_x)$ denotes a monotonically increasing regularization term that depends on the order of the nominal model n_x. The addition of the regularization term enables a rational tradeoff between model order and the worst-case performance associated with the robust controller.

Chapter 3

Model Order Selection

The aim of this chapter is to develop a robust-control-relevant model set and a model order selection procedure. In the development of the robust-control-relevant model set, defining the model structure is crucial. A suitable model structure is investigated in the first section. Thereafter, the identification procedure of the nominal model is investigated. In the third section, the robust-control-relevant model set is developed. A model order selection procedure is developed in the last section.

3.1 Model Structure

An uncertainty structure should be selected that enables the minimization of the worst-case performance $\mathcal{J}_{WC}(\mathcal{P}, C^{exp})$. To arrive at a suitable model structure, first, observe that the LFT based structure of the model set $\mathcal{P}$, Eq. (2.6), can be used to express the worst-case performance. Next, based on the LFT description and the experimental controller C^{exp} in conjunction with the weighting filters W and V, the weighted closed-loop matrix $\hat{M}$ is constructed in Figure 3.1.
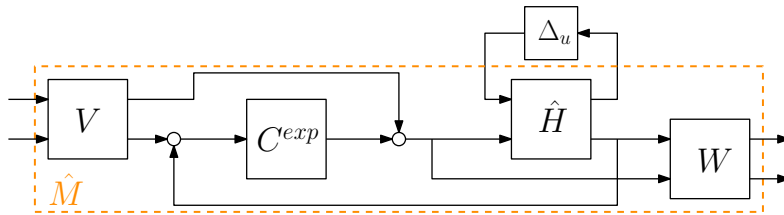
Figure 3.1 Block diagram of the weighted closed-loop.

Using the weighted closed-loop $\hat{M}$, the worst-case performance criterion is reformulated,

$$\mathcal{J}_{WC}(\mathcal{P}, C^{exp}) = \sup_{P \in \mathcal{P}^{dY}} \mathcal{J}(P, C^{exp}), \tag{3.1}$$

$$= \sup_{\|\Delta_u\|_\infty \leq \gamma} \left\| \mathcal{F}_u \left(\hat{M}(\hat{P}, C^{exp}), \Delta_u \right) \right\|_\infty, \tag{3.2}$$

$$= \sup_{\|\Delta_u\|_\infty \leq \gamma} \left\| \hat{M}_{22} + \hat{M}_{21} \Delta_u \left(I - \hat{M}_{11} \Delta_u \right)^{-1} \hat{M}_{12} \right\|_\infty. \tag{3.3}$$

The worst-case performance depends on the model uncertainty Δ_u in a complicated manner. Therefore, minimization of the worst-case performance $\mathcal{J}_{WC}(\mathcal{P}, C^{exp})$ over the model set $\mathcal{P}$ is

not immediately tractable. To enable the minimization of the worst-case performance, the model set is structured based on coprime factors. Therefore, the nominal model is structured as an Right Coprime Factorization (RCF).

Definition 3. Right Coprime Factorization (RCF). $\{N, D\}$ is an RCF of $\hat{P}$ if

1. $N, D \in \mathcal{RH}_\infty$;
2. Bezout identity holds, i.e. $\exists X, Y \in \mathcal{RH}_\infty$ s.t. $XD + YN = I$.

For a dual definition of an Left Coprime Factorization (LCF), see [68].

Also, to enable a tractable optimization problem, the experimental controller is also factorized as an RCF, $C^{exp} = N_c D_c^{-1}$.

Next, observe that the true system P_o is stabilized during experiments by the controller C^{exp}. Therefore, the true feedback-loop $T(P_o, C^{exp})$ should never be modelled by an unstable feedback-loop $T(\tilde{P}_u, C^{exp})$. Therefore, the systems $\tilde{P}_u$ that results in an unstable feedback-loop should be excluded from the model set. The exclusion of these systems results in a non-conservative model set, which enables high-performance motion control. Therefore, a model set should be selected that only parameterizes systems stabilized by the experimental controller C^{exp}. For this reason, the dual-Youla-Kučera structure is adopted. The key aspect of the dual-Youla-Kučera structure is that it only parameterizes systems stabilized by C^{exp} [4, 19, 14, 47, 43].

Definition 4. dual-Youla-Kučera model structure.

$$\mathcal{P}^{dY} = \left\{ P \middle| P = \left(\hat{N} + D_C \Delta_u \right) \left(\hat{D} - N_C \Delta_u \right)^{-1} \right\} \tag{3.4}$$

The dual-Youla-Kučera model structure can also be expressed as an LFT,

$$\hat{H}(\hat{P}, C^{exp}) = \left[\begin{array}{c|c} \hat{D}^{-1} N_C & \hat{D}^{-1} \\ \hline D_C + \hat{P} N_C & \hat{P} \end{array} \right]. \tag{3.5}$$

To arrive at an expression for the worst-case performance for the dual-Youla-Kučera model structure, the weighted closed-loop is expressed as an LFT [43, 47, 50, 12],

$$\hat{M}(\hat{P}, C^{exp}) = \left[\begin{array}{c|c} 0 & \left(\hat{D} + C^{exp} \hat{N} \right)^{-1} \begin{bmatrix} C^{exp} & I \end{bmatrix} V \\ \hline W \begin{bmatrix} D_C \\ -N_C \end{bmatrix} & WT(\hat{P}, C^{exp}) V \end{array} \right]. \tag{3.6}$$

Next, the worst-case performance criterion is rewritten to,

$$\mathcal{J}_{WC}(\mathcal{P}^{dY}, C^{exp}) = \sup_{P \in \mathcal{P}^{dY}} \mathcal{J}(P, C^{exp}), \tag{3.7}$$

$$= \sup_{\|\Delta_u\|_\infty \leq \gamma} \left\| \mathcal{F}_u \left(\hat{M}(\hat{P}, C^{exp}), \Delta_u \right) \right\|_\infty, \tag{3.8}$$

$$= \sup_{\|\Delta_u\|_\infty \leq \gamma} \left\| \hat{M}_{22} + \hat{M}_{21} \Delta_u \left(I - \hat{M}_{11} \Delta_u \right)^{-1} \hat{M}_{12} \right\|_\infty, \tag{3.9}$$

$$= \sup_{\|\Delta_u\|_\infty \leq \gamma} \left\| \hat{M}_{22} + \hat{M}_{21} \Delta_u \hat{M}_{12} \right\|_\infty, \tag{3.10}$$

$$\leq J(\hat{P}, C^{exp}) + \sup_{\|\Delta_u\|_\infty \leq \gamma} \left\| \hat{M}_{21} \Delta_u \hat{M}_{12} \right\|_\infty. \tag{3.11}$$

The inverse expression of the LFT, $\left(I - \hat{M}_{11}\Delta_u\right)^{-1}$, drops out since for this structure it holds that $\hat{M}_{11} = 0$. The inequality in Eq. (3.11) holds as $\hat{M}_{22} = J(\hat{P}, C^{exp})$. Furthermore, as the dual-Youla-Kučera model structure only parameterizes systems stabilized by C^{exp}, Eq. (3.10) is bounded [44]. In addition, this also means that for a finite uncertainty magnitude γ, the dual-Youla-Kučera model structure $\mathcal{P}^{dY}$ covers the true system P_o, i.e. $P_o \in \mathcal{P}^{dY}$.

However, direct minimization of $\mathcal{J}_{WC}(\mathcal{P}^{dY}, C^{exp})$ over the model set $\mathcal{P}^{dY}$ is still untractable because of the transfer matrices $\hat{M}_{21}$ and $\hat{M}_{12}$. These transfer matrices, complicate the connection between the magnitude of the model uncertainty, γ, and the worst-case performance, $\mathcal{J}_{WC}(\mathcal{P}^{dY}, C^{exp})$. To facilitate minimization of $\mathcal{J}_{WC}(\mathcal{P}^{dY}, C^{exp})$, observe that the RCFs of $\hat{P}$ and C^{exp} are not unique. In the next sections, this freedom is exploited to arrive at a transparent connection between the worst-case performance and the size of the model uncertainty.

3.2 Nominal Model

For the construction of the model set, defining the nominal model is crucial. Therefore, in this section, the nominal model and its identification procedure will be investigated.

3.2.1 Robust-Control-Relevant Nominal Model Identification

The nominal model should be selected such that it results in a small model set $\mathcal{P}$. Therefore, the nominal model $\hat{P}$ is identified in a robust-control-relevant manner with respect to P_o. Next, observe that the performance of the true system is related to the performance of any system P through,

$$\mathcal{J}(P_o, C) \le \mathcal{J}(P, C) + \|W\left(T(P_o, C) - T(P, C)\right)V\|_\infty. \tag{3.12}$$

The inequality follows from the triangular equality [51, 3]. Herein, the last term can be seen as the weighted mismatch between the candidate model P and the true system P_o. Therefore, evaluating Eq. (3.12) for the experimental controller C^{exp} results in the following identification criterion,

$$\hat{P} = \arg\min_P \|W\left(T(P_o, C^{exp}) - T(P, C^{exp})\right)V\|_\infty. \tag{3.13}$$

The main advantage of Eq. (3.13) is that the nominal model is identified with the weighting filters used for the synthesis of the robust controller. Taking the control objectives into account during the identification procedure results in a robust-control-relevant nominal model.

3.2.2 Coprime Factor Identification

The nominal model $\hat{P}$ is internally structured as an RCF to enable the construction of the dual-Youla-Kučera model structure. In this section, the non-uniqueness of the coprime factors is exploited to connect the identification procedure of the nominal model to the identification of the coprime factors.

The following definition is important for the upcoming derivations.

Definition 5. The pair $\left\{\tilde{N}_e, \tilde{D}_e\right\}$ is an Left Coprime Factorization (LCF) with co-inner numerator of $\begin{bmatrix} C^{exp}V_2 & V_1 \end{bmatrix}$, if it is an LCF of $\begin{bmatrix} C^{exp}V_2 & V_1 \end{bmatrix}$ and in addition, $\tilde{N}_e^H \tilde{N}_e = I$.

The existence of the LCF with co-inner numerator is guaranteed [43].

Next, consider the following definition, which provides a connection between the identification of the nominal model and the identification of the coprime factors by the development of a new pair of coprime factors.

Theorem 1. Coprime Identification Criterion. Let $\left\{\tilde{N}_e, \tilde{D}_e\right\}$ be an LCF of $\left[C^{exp}V_2 \quad V_1\right]$, with $\tilde{N}_e^* \tilde{N}_e = I$ and $\tilde{N}_e = \left[\tilde{N}_{e,2} \quad \tilde{N}_{e,1}\right]$. Then the identification criterion in Eq. (3.13) is equivalent to,

$$\min_{\hat{N},\hat{D}} \left\| W \left(\begin{bmatrix} N_o \\ D_o \end{bmatrix} - \begin{bmatrix} \hat{N} \\ \hat{D} \end{bmatrix} \right) \right\|_\infty, \quad \hat{N}, \hat{D} \in \mathcal{RH}_\infty. \tag{3.14}$$

Where,

$$\begin{bmatrix} \hat{N} \\ \hat{D} \end{bmatrix} = \begin{bmatrix} \hat{P} \\ I \end{bmatrix} \left(\tilde{D}_e + \tilde{N}_{e,2} V_2^{-1} \hat{P} \right)^{-1}, \qquad \begin{bmatrix} N_o \\ D_o \end{bmatrix} = \begin{bmatrix} P_o \\ I \end{bmatrix} \left(\tilde{D}_e + \tilde{N}_{e,2} V_2^{-1} P_o \right)^{-1}. \tag{3.15}$$

A proof is given in [43, Theorem 1], [42, Proposition 2].

It can be seen that the optimization criterion is reduced from a four-block problem, Eq. (3.13), to a two-block problem, Eq. (3.14). This is achieved as the $\mathcal{H}_\infty$-norm is invariant for the pre-multiplication of a matrix with an inner numerator and the post-multiplication of a matrix with a co-inner numerator. Using the new coprime factorization, the robust-control-relevant model set is constructed in the next section.

3.3 Robust-Control-Relevant Model Structure

In this section, the model structure is completed such that identification of the nominal model and the size of the uncertainty together aim at the minimization of the worst-case performance. Therefore, the coprime factorization introduced in the previous section is adopted, and a new coprime factorization of the experimental controller developed in the next definition.

Definition 6. Robust-Control-Relevant RCF of the experimental controller. The pair $\{N_C, D_C\}$ is a (W_u, W_y)-normalized RCF if it satisfies Definition 3 and,

$$\begin{bmatrix} W_u N_C \\ W_y D_C \end{bmatrix}^H \begin{bmatrix} W_u N_C \\ W_y D_C \end{bmatrix} = I. \tag{3.16}$$

Using the new coprime factorizations in Theorem 1 and Definition 6, the robust-control-relevant model set is defined.

Definition 7. Robust-Control-Relevant Model Set. Given the robust-control-relevant RCF of $\hat{P}, \left\{\hat{N}, \hat{D}\right\}$ according to Theorem 1, robust-control-relevant RCF of $C^{exp}, \{N_C, D_C\}$ according to Definition 6. Then the robust-control-relevant model set is defined as,

$$\mathcal{P}^{RCR} = \left\{ P \middle| P = \left(\hat{N} + D_C \Delta_u \right) \left(\hat{D} - N_C \Delta_u \right)^{-1} \right\}. \tag{3.17}$$

The key advantage of the robust-control-relevant model set is the direct relationship between the worst-case performance, the nominal performance and the size of the uncertainty as shown

in the following derivation,

$$\mathcal{J}_{WC}(\mathcal{P}^{RCR}, C^{exp}) = \sup_{\|\Delta_u\|_\infty \le \gamma} \left\| \mathcal{F}_u \left(\hat{M}^{RCR}(\hat{P}, C^{exp}), \Delta_u \right) \right\|_\infty, \tag{3.18}$$

$$= \sup_{\|\Delta_u\|_\infty \le \gamma} \left\| \hat{M}_{22}^{RCR} + \hat{M}_{21}^{RCR} \Delta_u \hat{M}_{12}^{RCR} \right\|_\infty, \tag{3.19}$$

$$\le J(\hat{P}, C^{exp}) + \sup_{\|\Delta_u\|_\infty \le \gamma} \left\| \hat{M}_{21}^{RCR} \Delta_u \hat{M}_{12}^{RCR} \right\|_\infty, \tag{3.20}$$

$$= J(\hat{P}, C^{exp}) + \gamma. \tag{3.21}$$

In contrast to Eq. (3.11), the transfer matrices $\hat{M}_{21}^{RCR}$ and $\hat{M}_{12}^{RCR}$ do not influence the bound in Eq. (3.21), see [43, Theorem 9] for a proof. It can be seen that the worst-case performance $\mathcal{J}_{WC}(\mathcal{P}^{dY}, C^{exp})$ is now directly related to the performance of the nominal model and the magnitude of the model uncertainty.

Furthermore, the size of the model uncertainty, γ, is minimized during the identification of the nominal model. In fact, the identification criterion, Eq. (3.13), is equal to γ. Hence, the identification of the nominal model results in the minimal size of the model uncertainty γ. Consequently, the selected model structure in combination with the nominal model identification approach together aim at minimizing the worst-case performance Eq. (2.12). For this reason, the considered model set is robust control relevant.

Furthermore, the proposed model structure allows the usage of an unstructured model uncertainty, which results in a non-conservative robust controller synthesis. This is in contrast to existing methods regarding system identification for control where structured model uncertainties are considered which creates conservatism in the robust controller synthesis [15, 60].

3.4 Order Selection Rule

In this section, a model order selection procedure is developed which breaks the tradeoff between the performance of the system with a robust controller and the order of the nominal model. Therefore, deriving a connection between the worst-case performance, Eq. (2.11), the robust-control-relevant nominal model identification criterion and the size of the uncertainty is essential.

As mentioned in Section 2.2.1, in this research, the concept of a regularization term as considered in the prediction error framework is used for the selection of the model order, see [56] and references therein. Three commonly used order selection criteria are i) Bayesian information criterion rule [52], ii) generalized information criterion rule [34] and iii) Akaike information criterion rule [2]. Essentially, these order selection rules penalize model order by adding a regularization term which depends linearly on the model order. In this research, a similar regularization term is adopted by considering a regularization term that depends linearly on the model order,

$$n_x^* = \arg\min_{n_x} \mathcal{J}_{WC}(\mathcal{P}(n_x), C_{exp}) + \phi n_x, \text{ s.t. } P_o \in \mathcal{P}(n_x). \tag{3.22}$$

Herein, the constant ϕ is a non-negative tuning parameter. The value of this parameter may be adjusted based on the selected parametrization, the considered system, and the required performance. A possibility on how to select the value of the tuning parameter ϕ will be discussed in a simulation example in Chapter 7. The computation of the worst-case performance, $\mathcal{J}_{WC}(\mathcal{P}(n_x), C_{exp})$, is essentially a skewed Structured Singular Value (SSV) problem, which

requires a large computational effort. In addition, the connection with the identification procedure is unclear. Therefore, in the next theorem, an overbound of the worst-case performance, $\mathcal{J}_{WC}(\mathcal{P}(n_x), C_{exp})$, is derived, which reduces the computational effort, and provides a transparent connection between the identification criterion of the nominal model and the worst-case performance.

Theorem 2. Given the robust-control-relevant model set $\mathcal{P}^{RCR}$ according to Definition 7, with a nominal model of order n_x. Then,

$$\mathcal{J}_{WC}(\mathcal{P}^{RCR}(n_x), C^{exp}) \leq \mathcal{J}(P_o, C^{exp}) + 2\gamma(n_x). \tag{3.23}$$

A proof is given in Appendix B.1.

This theorem states that the worst-case performance of the control-relevant-model set is bounded by the performance of the true system and the size of the uncertainty γ. Therefore, this bound depends on the selected order n_x only through the size of the model uncertainty. Notice that γ is minimized during the identification of the nominal model. Next, Eq. (3.22) and Theorem 2 are combined to arrive at the definition of the optimal model order n_x^*.

Definition 8. Model order selection rule. Given the robust-control-relevant model structure $\mathcal{P}^{RCR}$ according to Definition 7. Then the model order selection rule is defined as

$$n_x^* = \arg\min_{n_x} \mathcal{W}(n_x). \tag{3.24}$$

Where the cost function $\mathcal{W}(n_x)$ is defined as

$$\mathcal{W}(n_x) = \gamma(n_x) + \tilde{\phi} n_x. \tag{3.25}$$

Combining the model structure, nominal model identification procedure and the model order selection rule, constitutes a framework that enables the synthesis of low-order robust controllers that achieve a high performance. The model order selection procedure extends to existing methods regarding system identification for robust control where typically high model orders are selected which hampers successful implementation in a real-time environment [60, 47].

3.5 Overview

The main contributions of this chapter are twofold, (i) developing a robust-control-relevant model structure, (ii) developing a model order selection procedure. Regarding (i), to construct a non-conservative model set, the dual-Youla-Kučera plays an important role. More specifically, the freedom in the coprime factors that constitute the dual-Youla-Kučera model structure are exploited in the second section to facilitate a transparent connection between the worst-case performance, the nominal performance and the size of the model uncertainty. Based on the proposed model structure in conjunction with the identification approach of the nominal model, a tractable identification procedure is derived. Furthermore, the proposed model structure allows the usage of an unstructured model uncertainty, which results in a non-conservative robust controller synthesis. This is in contrast to existing methods regarding system identification for control where structured perturbation blocks are considered which creates conservatism in the robust controller synthesis [15, 60].

Regarding (ii), a model order selection procedure is developed in the third section. To arrive at a suitable model order selection procedure, a novel connection between the performance and the selected model order is derived. In addition, the regularization term which accounts for the addition of the model order is specified based on findings in the literature. The regularization term in conjunction with the novel connection enables to break the tradeoff between model order and the performance of the resulting robust controller. The model order selection procedure extends to existing methods regarding system identification for robust control where typically high model orders are selected which hampers successful implementation in a real-time environment [60, 47].

Chapter 4

Parametrization

In this chapter, a parametrization of the nominal model is developed that enables (i) the model order selection procedure, (ii) numerically reliable synthesis of the nominal model. To enable (i), the parametrization should, for a given model order, describe a rich class of mechanical systems. Therefore, in the first section, the class of mechanical systems is investigated. In the second section, a parametrization is developed that enables (i) and (ii). To indicate the class of systems the proposed parametrization describes, an example will be given in the third section. An overview of this chapter is given in the last section.

4.1 Mechanical System Class

The parametrization should enable the model selection procedure. Hence, for a given model order, the parametrization should describe a sufficiently rich class of mechanical systems. For this reason, the class of mechanical systems is investigated in this section.

4.1.1 Mechanical Systems

In order to come up with a parametrization that describes mechanical systems, the class of mechanical systems needs to be defined first. Therefore, the dynamic behaviour of mechanical systems is investigated using Newton's second law,

$$M\ddot{q}(t) + D\dot{q}(t) + Kq(t) = u(t). \tag{4.1}$$

Herein, $M \in \mathbb{R}^{n_m \times n_m}$, $D \in \mathbb{R}^{n_m \times n_m}$ and $K \in \mathbb{R}^{n_m \times n_m}$ denote the mass-, damping- and stiffness-matrix, where n_m denotes the number of modal coordinates [16]. An essential step in the analysis of mechanical systems is to evaluate its modal form. Therefore, consider the undamped generalized eigenvalue problem,

$$(\omega_k^2 M - K)u_{O,k} = 0. \tag{4.2}$$

Where ω_k denotes the k-th undamped eigenfrequency and $u_{O,k}$ denotes the k-th undamped eigenmode. The eigenvalues are nonnegative real numbers, i,e. $\omega_k \geq 0$. Rigid-body modes correspond to those eigenfrequencies equal to zero. The origin of these modes is found in the rank deficiency of the stiffness matrix K, therefore, $\dim(\ker(K)) = n_o$. Physically, a rigid-body mode can be interpreted as a free change in translation or rotation without deformation.

To arrive at the modal form, the undamped eigenmodes are stacked in the matrix U_O and are normalized with respect to the mass, hence, $U_O^\top M U_O = I$ and $U_O^\top M U_O = \Omega^2$. Next, consider

the generalized coordinates $q_m = U_O^{-1} q$ and the corresponding generalized equations of motion,

$$\ddot{q}_m + \underbrace{U_O^\top D U_O}_{D_m} \dot{q}_m + \Omega^2 q_m = U_O^\top u. \tag{4.3}$$

For many motion system, the modal damping matrix is a full matrix, which results in a coupled set of second-order differential equations. This type class of mechanical systems is also referred to as the generally damped mechanical system class, which is formally defined as follows.

Definition 9. Generally damped mechanical system.

$$\Phi_{gd} = \left\{ \left[\begin{array}{cc|c} O & I & o \\ -\Omega^2 & -D_m & \mathcal{R} \\ \hline \mathcal{L} & o & \end{array} \right] \middle| \begin{array}{ccc} \mathcal{L} \in \mathbb{R}^{n_y \times n_m} & \mathcal{R} \in \mathbb{R}^{n_m \times n_u} & D_m \in \mathbb{R}^{n_m \times n_m} \\ \Omega^2 \in \mathbb{R}^{n_m \times n_u} \end{array} \right\} \tag{4.4}$$

High precision motion systems are typically lightly damped. This often results in a diagonal modal damping matrix, $D_m = \mathrm{diag}(d_{m,i})$, resulting in a decoupled set of second-order differential equations. This type of damping is referred to as proportionally damped which is formally defined below.

Definition 10. Proportionally damped mechanical system.

$$\Phi_{pd} = \{\phi \in \Phi_{gd} | D_m = \mathrm{diag}(d_{m,i}), \ i \in \{1, ..., n_m\}\} \tag{4.5}$$

Recent developments in the design of motion stages resulted in the proportional damping assumption being invalid for motion stages [28, 63]. Therefore, in this research, a parametrization is developed that encompasses both the generally damped and proportionally damped system class.

4.1.2 Structural Properties

In this section, the structural properties of motion systems are investigated. This enables the formulation of constraints on the parametrization which are particularly relevant for the identification of mechanical systems.

Rigid-Body Mode

As discussed in Section 4.1.1, motion systems typically contain rigid-body modes. A rigid-body mode is a free change in translation or rotation without deformation. These rigid-body modes typically dominate the frequency response in the low-frequency range, whereas the flexible dynamics are often more pronounced in the high-frequency region. Prescribing the number of rigid-body modes is particularly relevant for the identification of mechanical systems. A rigid-body mode is formally defined in the definition below.

Definition 11. rigid-body Mode. Given a generally damped mechanical system $\Sigma \in \Phi_{gd}$. A rigid-body mode is defined as the vector that spans the kernel of the stiffness matrix K, $\mathrm{span}\{v_1, ..., v_{n_o}\} = \ker(K)$. The number of rigid-body modes equals $n_0 = \dim(\ker(K))$.

Order Increments

For successful and efficient order selection, determining the relevant orders for mechanical systems is crucial. If a state-space realization is minimal, the McMillan degree is equal to the

number of states. If a mechanical system is considered which uses position measurement and force actuation, then the McMillan degree is defined as

$$n_x = 2n_m. \tag{4.6}$$

As a result, for controllable and observable mechanical systems, the McMillan degree is an even number and the order increment is therefore 2.

Relative Degree

An important input-output property of a system is the relative degree.

Definition 12. Relative degree. Given an input $y \in \mathbb{R}^{n_y}$ and an output $u \in \mathbb{R}^{n_u}$. Let κ_i be the minimum order of the time derivative of output y_i which is affected directly by input u_j. Then the relative degree of output y_i is defined as κ_i [32].

Motion systems are often controlled using position sensors and acceleration-actuators, therefore, the following constraint on the relative degree should be satisfied.

Theorem 3. Given a mechanical system $\Phi \in \Phi_{gd}$, then the following inequality holds for the relative degree,

$$\kappa_i \geq 2, \text{ for } i = 1, ..., n_y. \tag{4.7}$$

A proof is given in Appendix B.2.

Therefore, the parametrization should be able to describe systems with at least a relative degree of 2.

4.2 Parametrization

In system identification, often a common denominator parametrization is considered. This approach is first introduced to SISO systems, and later extended to Multiple Input Multiple Output (MIMO) systems [5]. A major drawback of the common denominator parametrization is that for a given order, the parametrization can only describe a limited class of systems [65]. Another often used parametrization for MIMO systems is the full-Matrix Fraction Description (MFD) [55]. For a given order, the full-MFD approach is able to describe a much richer class of systems. In addition, numerical reliable synthesis methods are available for this parametrization. However, the minimal order-increment with which the order of the full-MFD can be increased is n_u [65, Section 2.3.5]. As next-generation motion systems contain many inputs and outputs, this increment is large which may result in unnecessarily large model orders. This is undesirable in terms of numerical conditioning and the order of the resulting robust controller.

In this research, a parsimonious MFD parametrization is developed [17, 62]. Through the usage of pseudo-canonical indices, a large class of systems can be parameterized for a given order of the nominal model. In addition, the developed parametrization enables the usage of well-established identification algorithms, including Sanathanan and Koerner (SK) and Gauss-Newton (GN). To enhance numerical reliability, the number of parameters of the nominal model is kept to a minimum by incorporating mechanical properties through trivial parameter constraints.

4.2.1 Pseudo-Canonical Form

In this section, an MFD parametrization is developed that enables the parametrization of both generally damped and proportionally damped systems. To arrive at a suitable parametrization, first, consider the class of strictly proper systems,

$$\Phi_p = \left\{ \left[\begin{array}{c|c} A & B \\ \hline C & \end{array} \right] \middle| \middle| \right\}. \tag{4.8}$$

Related to the state-space parametrization, the following matrices are defined [32],

$$\mathcal{O} = \begin{bmatrix} C \\ CA \\ \vdots \\ CA^{n_x-1} \end{bmatrix}, \qquad \mathcal{C} = \begin{bmatrix} B & AB & \dots & A^{n_x-1}B \end{bmatrix}. \tag{4.9}$$

Herein, $\mathcal{O}$ denotes the observability matrix and $\mathcal{C}$ denotes the controllability matrix. Next, a system $\phi \in \Phi_p$ is observable or controllable if $\mathcal{O}$ or $\mathcal{C}$ has full rank. An important concept for the construction of the pseudo-canonical form is the similarity transformation.

Definition 13. Similarity transformation. Given a matrix $T = \{T \in \mathbb{R}^{n_x \times n_x} | \text{rank}(T) = n_x\}$. Next, given the original coordinate frame x, and the transformed state coordinate frame $\tilde{x} = Tx$ [29]. Then the transformed system equals,

$$\left[\begin{array}{c|c} A & B \\ \hline C & \end{array} \right] \xrightarrow{T} \left[\begin{array}{c|c} TAT^{-1} & TB \\ \hline CT^{-1} & \end{array} \right]. \tag{4.10}$$

By selecting n_x rows of the observability matrix, or n_x columns of the controllability matrix that constitute an invertible matrix, a similarity transformation matrix is obtained that is able to transform a system into a pseudo-canonical form. This is a key concept in the parametrization of MIMO systems with MFDs.

Next, the process of selecting the rows of $\mathcal{O}$ or the columns of $\mathcal{C}$ is formalized. Therefore, consider the observability matrix with respect to the i-th row of C and the controllability matrix with respect to the i-th column of B,

$$\mathcal{O}_{\eta_i} = \begin{bmatrix} [C]_i \\ [C]_i A \\ \vdots \\ [C]_i A^{\eta_i-1} \end{bmatrix} \in \mathbb{R}^{\eta_i \times n_x}, \quad \mathcal{C}_{\mu_i} = \begin{bmatrix} [B]^i & A[B]^i & \dots & A^{\mu_i-1}[B]^i \end{bmatrix} \in \mathbb{R}^{n_x \times \mu_i}. \tag{4.11}$$

Herein, η_i and μ_i denote the pseudo-canonical observability (p.c.o.) and pseudo-canonical controllability (p.c.c.) index respectively [53]. A similarity transformation matrix is constructed by stacking the rows of O_{η_i} and the columns of $\mathcal{C}_{\mu_i}$,

$$\mathcal{O}_r = \begin{bmatrix} \mathcal{O}_{\eta_1} \\ \vdots \\ \mathcal{O}_{\eta_{n_y}} \end{bmatrix} \in \mathbb{R}^{n_x \times n_x}, \qquad \mathcal{C}_r = \begin{bmatrix} \mathcal{C}_{\mu_1} & \dots & \mathcal{C}_{\mu_{n_y}} \end{bmatrix} \in \mathbb{R}^{n_x \times n_x}. \tag{4.12}$$

An observable system can be transformed into a pseudo-canonical observable form using the similarity transformation matrix Eq. (4.12),

$$\left[\begin{array}{c|c} A_o & B_o \\ \hline C_o & \end{array}\right] = \left[\begin{array}{c|c} \mathcal{O}_r^{-1}A\mathcal{O}_r & \mathcal{O}_r^{-1}B \\ \hline C\mathcal{O}_r & \end{array}\right]. \tag{4.13}$$

Analogously, a controllable system can be transformed into a pseudo-canonical controllable form using the similarity transformation matrix Eq. (4.12),

$$\left[\begin{array}{c|c} A_c & B_c \\ \hline C_c & \end{array}\right] = \left[\begin{array}{c|c} \mathcal{C}_r^{-1}A\mathcal{C}_r & \mathcal{C}_r^{-1}B \\ \hline C\mathcal{C}_r & \end{array}\right]. \tag{4.14}$$

However, for a similarity transformation to be valid, the similarity matrix, $\mathcal{O}_r$ or $\mathcal{C}_r$, must be invertible. Therefore, the rows of the observability and the columns of the controllability matrix must be selected such that they constitute a set of linearly independent rows or columns. For this reason, the p.c.o. and p.c.c. need to be admissible. The admissible set of p.c.o. and p.c.c. indices are defined in the following definitions [10, 53, 21].

Definition 14. Admissible pseudo-canonical observability (p.c.o.) indices. The admissible set of p.c.o. indices is given by

$$\Gamma = \left\{ \gamma = \begin{bmatrix} \eta_1 & \dots & \eta_{n_y} \end{bmatrix} \, \middle| \, \sum_{i=1}^{n_y} \eta_i = n_x, \ \ \eta_1 \geq \dots \geq \eta_{n_y} \geq 0, \ \ \mathrm{rank}(\mathcal{O}_r) = n_x \right\}. \tag{4.15}$$

Definition 15. Admissible pseudo-canonical controllability (p.c.c.) indices. The set of admissible p.c.c. indices is given by

$$\Delta = \left\{ \delta = \begin{bmatrix} \mu_1 & \dots & \mu_{n_u} \end{bmatrix} \, \middle| \, \sum_{i=1}^{n_u} \mu_i = n_x, \ \ \mu_1 \geq \dots \geq \mu_{n_u} \geq 0, \ \ \mathrm{rank}(\mathcal{C}_r) = n_x \right\}. \tag{4.16}$$

4.2.2 Right Matrix Fraction Description Parametrization

In this subsection, a Right Matrix Fraction Description (RMFD) parametrization is defined using the definition of the pseudo-canonical indices, that enables parametrization of generally damped and proportionally damped systems. To arrive at the parametrization, first, consider the formal definition of the RMFD.

Definition 16. Right Matrix Fraction Description. Given $B(s) \in \mathbb{C}^{n_y \times n_u}$ and $A(s) \in \mathbb{C}^{n_u \times n_u}$, then

$$P(s) = B(s)A^{-1}(s) \tag{4.17}$$

For a more extensive definition and the definition of the Left Matrix Fraction Description (LMFD), see [31].

Next, the RMFD parametrization is defined, based on the p.c.c. indices of Definition 15.

Definition 17. Strictly proper pseudo-canonical Right Matrix Fraction Description (RMFD) parametrization. Given an admissible set of p.c.c. indices $\delta \in \Delta$, for which the following holds,

$$v_j = \max\left(\mu_{max} - 1, \mu_j\right), \ \ \mu_i \geq \nu_i, \ i \in \{1, ..., n_u\}. \tag{4.18}$$

Then, the parametrization is defined as

$$[A(s,\theta)]_i^j = \delta_{ij}s^{\mu_i} - \sum_{k=1}^{\mu_i} \alpha_{jik}s^{k-1}, \quad \text{for } i,j \in \{1,...,n_u\}, \tag{4.19}$$

$$[B(s,\theta)]_i^j = \sum_{k=1}^{\nu_j} \beta_{jik}s^{k-1}, \quad \text{for } \begin{cases} i \in \{1,...,n_y\}, \\ j \in \{1,...,n_u\}. \end{cases} \tag{4.20}$$

The parameter vector θ is defined as

$$\theta = \begin{bmatrix} \theta_1 & ... & \theta_{n_u} \end{bmatrix}^\top \qquad\qquad \theta_j = \begin{bmatrix} \alpha_j \\ \beta_j \end{bmatrix} \tag{4.21}$$

$$\alpha_j = \begin{bmatrix} \alpha_{j11} & ... & \alpha_{j1\mu_1} & \big| & \alpha_{j21} & ... & \alpha_{j2\mu_2} & \big| & ... & \big| & \alpha_{jn_u1} & ... & \alpha_{jn_u\mu_{n_u}} \end{bmatrix}^\top, \tag{4.22}$$

$$\beta_j = \begin{bmatrix} \beta_{j11} & ... & \beta_{j1\nu_j} & \big| & \beta_{j21} & ... & \beta_{j2\nu_j} & \big| & ... & \big| & \beta_{jn_y1} & ... & \beta_{jn_y\nu_j} \end{bmatrix}^\top. \tag{4.23}$$

This parametrization essentially is a dual parametrization to LMFD parametrization in [18, Section 4.3.2]. The constraint on the p.c.c. indices, Eq. (4.18), ensures that the RMFD is strictly proper without having to enforce nontrivial parameter constraints on the parameter vector θ [25, 18]. To understand the proposed parametrization, consider the following example.

Example 1. Given $n_u = n_y = 2$ and an admissible set of p.c.c. indices $\delta = \{3,2\}$. The corresponding parametrization is defined as

$$A(s,\theta) = \begin{bmatrix} s^3 - \alpha_{113}s^2 - \alpha_{112}s - \alpha_{111} & -\alpha_{213}s^2 - \alpha_{212}s^1 - \alpha_{211} \\ -\alpha_{122}s - \alpha_{121} & s^2 - \alpha_{222}s - \alpha_{221} \end{bmatrix}, \tag{4.24}$$

$$B(s,\theta) = \begin{bmatrix} \beta_{112}s + \beta_{111} & \beta_{212}s + \beta_{211} \\ \beta_{122}s + \beta_{121} & \beta_{222}s + \beta_{221} \end{bmatrix}. \tag{4.25}$$

4.2.3   Mechanical Properties

In this section, the relative degree and rigid-body modes, described in Section 4.1.1, will be enforced through trivial parameter constraints. First, the relative degree constraint is investigated, thereafter, enforcing the rigid-body modes is investigated.

Relative Degree

In this section, a relative degree greater than or equal to two is enforced by considering a constraint on the p.c.c. indices. This is formally discussed in the following theorem.

Theorem 4. Relative Degree. Given an admissible set of p.c.c. indices, $\delta \in \Delta$. Then, a relative degree, $\kappa_i \geq 2$ is enforced by lowering the indices of the numerator matrix,

$$v_i = \max\left(\mu_{max} - 1, \mu_i\right) - 1, \qquad\qquad \mu_i \geq \nu_i. \tag{4.26}$$

A proof in provided in Appendix B.3

Essentially, this theorem states that to enforce a relative degree greater than or equal to two, the polynomial degree of the numerator matrix must be lowered by 1.

Rigid-Body Modes

In this section, a parameter constraint is proposed to enforce rigid-body modes. The parameter constraint is formally defined in the following theorem.

Theorem 5. Rigid-body modes constraint. Given $\mu_i \geq 2$, $\forall i = 1, ..., n_u$ and let the number of rigid-body modes be defined as $n_o = n_u$. Then, n_o rigid-body modes are enforced by the following parameter constraint,

$$\alpha_{ijk} = 0, \ \forall i = 1, ..., n_o, \ j = 1, ..., n_o, \ k = 1, 2. \tag{4.27}$$

A proof is given in [18, Appendix E.12].

Using Theorem 5, rigid-body modes can be enforced by means of a trivial parameter constraint. If the number of inputs exceeds the number of rigid-body modes, one might consider alternative constraints as shown in [18, Theorem 11]. To elucidate the constraints regarding the number of rigid-body modes and a relative degree larger than 1, consider the following example.

Example 2. Given $n_u = n_y = 2$, an admissible set of p.c.c. indices $\delta = \{3, 2\}$, the number of rigid-body modes $n_o = 2$ and a relative degree larger than 1. The corresponding parametrization is defined as

$$A(s, \theta) = \begin{bmatrix} s^3 - \alpha_{113}s^2 & -\alpha_{213}s^2 \\ 0 & s^2 \end{bmatrix}, \tag{4.28}$$

$$B(s, \theta) = \begin{bmatrix} \beta_{111} & \beta_{211} \\ \beta_{121} & \beta_{221} \end{bmatrix}. \tag{4.29}$$

4.2.4 Indices

In this subsection, the selection of a suitable p.c.c. index set is investigated. Ideally, the p.c.c. indices should satisfy the relative degree constraint, Theorem 4. To arrive at a p.c.c. index set that satisfies the relative degree constraint, first consider a set of admissible p.c.c. indices,

$$\delta = \begin{bmatrix} \mu_{max} & \mu_1 & \ldots & \mu_{n_y} \end{bmatrix}. \tag{4.30}$$

Next, using the relative degree constraint on the numerator, $v_i = \max(\mu_{max} - 1, \mu_i) - 1$, the numerator indices are defined as

$$\begin{bmatrix} \nu_1 & \ldots & \nu_{n_u} \end{bmatrix} = \begin{bmatrix} \mu_{max} & \mu_{max} - 1 & \ldots & \mu_{max} - 1 \end{bmatrix}. \tag{4.31}$$

For the parametrization to have a relative degree greater than or equal to two, recall the following constraint on the p.c.c. indices,

$$\mu_i \geq \nu_i, \ \text{for } i = 1, ..., n_u. \tag{4.32}$$

For this reason, combining Eq. (4.30) and Eq. (4.31) with Eq. (4.32), results in the following constraint on the p.c.c. indices,

$$\mu_i \geq \mu_{max} - 2. \tag{4.33}$$

An index set that satisfies the relative degree constraint, Eq. (4.33), is the so-called generic controllability index [23]. The generic controllability index is formally defined in the following definition.

Definition 18. Generic controllability index. The generic controllability index, δ_g, is defined as

$$\delta_g = \{\delta \in \Delta \,||\mu_i - \mu_j| = 0 \vee 1, \; i, j \in \{1, ..., n_u\}\}. \tag{4.34}$$

Observe that for generic indices, the similarity matrix, $\mathcal{C}_r$ is defined as the first n_x columns of $\mathcal{C}$. As a result, the generic controllability indices are admissible if,

$$\text{rank}(\mathcal{C}_g) = n_x. \tag{4.35}$$

In addition, the generic indices are also canonical indices, more specifically, Kronecker indices [1]. The resulting parametrization is in literature also referred to as the polynomial Echelon form or Popov canonical form, [23, 31, 65].

Example 3. Given $n_y = n_u = 4$, $n_x = 20$, then the corresponding set of specific indices is defined as

$$\delta_g = \{5, 5, 5, 5\}. \tag{4.36}$$

Example 4. Given $n_y = n_u = 4$, $n_x = 22$, then the corresponding set of specific indices is defined as

$$\delta_g = \{6, 6, 5, 5\}. \tag{4.37}$$

For generally damped systems it holds that generic indices are generically equivalent to generally damped systems [18, Theorem 8]. However, this does not mean that all mechanical systems can be described by means of generic indices. This will be shown by means of an example in Section 4.3. First, consider the following theorem.

Theorem 6. Given $\frac{n_x}{n_u} \in \mathbb{Z}$ and $\mathcal{C}_g$ the generic observability matrix. Let $\bar{\mathcal{C}}_g$ be the generic observability matrix based on a similarity, input or output transformation of $\mathcal{C}_g$ [29]. Then,

$$\text{rank}\left(\bar{\mathcal{C}}_g\right) = \text{rank}\left(\mathcal{C}_g\right). \tag{4.38}$$

A proof is given in Appendix B.4.

This theorem essentially states that given a state-space representation of a system $\phi \in \Phi_{gd}$ for which it holds that $\text{rank}(\mathcal{C}_g) < n_x$, the system ϕ cannot be described with generic indices.

An alternative to the generic controllability index set is the so-called specific controllability index. This index is formally defined in the following definition.

Definition 19. Specific controllability index. The specific controllability index is defined as

$$\delta_s = \{\delta \in \Delta \,||\mu_i - \mu_j| = 0 \vee 2, \; i, j \in \{1, ..., n_u\}\}. \tag{4.39}$$

Next, consider the following examples.

Example 5. Given $n_y = n_u = 4$, $n_x = 20$, then the corresponding set of specific indices is defined as

$$\delta_s = \{6, 6, 4, 4\}. \tag{4.40}$$

Example 6. Given $n_y = n_u = 4$, $n_x = 22$, then the corresponding set of specific indices is defined as

$$\delta_s = \{6, 6, 6, 4\}. \tag{4.41}$$

For a specific choice of p.c.c. indices, it is known that the resulting parametrization does not cover each controllable system [21, 27]. For this reason, it is important to understand which class of mechanical systems the RMFD parametrization covers using generic or specific indices. To this end, consider the following theorem.

Theorem 7. Consider a MIMO system with the following decoupled structure,

$$P(s) = \begin{bmatrix} P_1(s) & & O \\ & \ddots & \\ O & & P_{n_u}(s) \end{bmatrix}, \tag{4.42}$$

where, $P_i(s)$ denotes the i-th SISO with a McMillan degree $n_{x,i}$. Next, the individual transfer functions are ordered such that $n_{x,1} \geq n_{x,2} \geq ... \geq n_{x,n_u}$. Then the following holds,

1. If, $|n_{x,i} - n_{x,j}| = 0 \vee 1$, $i, j \in \{1, ..., n_u\}$, then the system can be described using generic indices.

2. If, $|n_{x,i} - n_{x,j}| = 0 \vee 2$, $i, j \in \{1, ..., n_u\}$, then the system can be described using specific indices.

Therefore, from Theorem 7, it is concluded that there exist systems at which a description by means of generic indices is more desirable than specific indices and vice versa. On the other hand, there exist systems that can be described by means of generic and specific indices. This will be investigated in the next section by means of an example.

4.3 Mechanical Example

In this subsection, a mechanical example will be given to clarify the choice between generic and specific indices. Consider the mechanical system presented in Figure 4.1.
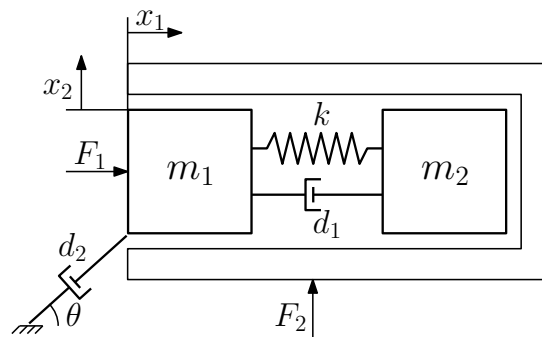

Figure 4.1 Free body diagram of the mechanical system.

The system consists of two point masses, m_1 and m_2. These masses are connected through a spring with stiffness k and a damper with a damping constant d_1. The horizontal position of the

first mass is indicated by x_1. The vertical position of both masses is indicated by x_2. The system is actuated in the horizontal direction by a force F_1 and in the vertical direction by a force F_2. A diagonal damper is connected to the mass m_1 under an angle θ. In the next paragraph, the selection of the p.c.c. indices will be investigated with and without the damper d_2.

Proportional Damping

First, consider the mechanical system without a diagonal damper, e.i. $d_2 = 0$. As a result, the MIMO system is fully decoupled, therefore, the system is proportionally damped. Next, consider the corresponding state-space parametrization,

$$
A = \begin{bmatrix}
0 & 1 & 0 & 0 & 0 & 0 \\
-\frac{k_1}{m_1} & -\frac{d_1}{m_1} & \frac{k_1}{m_1} & \frac{d_1}{m_1} & 0 & 0 \\
0 & 0 & 0 & 1 & 0 & 0 \\
\frac{k_1}{m_2} & \frac{d_1}{m_2} & -\frac{k_1}{m_2} & -\frac{d_1}{m_2} & 0 & 0 \\
0 & 0 & 0 & 0 & 0 & 1 \\
0 & 0 & 0 & 0 & -\frac{k_2}{m_1+m_2} & -\frac{d_2}{m_1+m_2}
\end{bmatrix}
\tag{4.43}
$$

$$
B = \begin{bmatrix}
0 & 0 \\
\frac{1}{m_1} & 0 \\
0 & 0 \\
0 & 0 \\
0 & 0 \\
0 & \frac{1}{m_1+m_2}
\end{bmatrix}
\qquad
C = \begin{bmatrix}
1 & 0 & 0 & 0 & 0 & 0 \\
0 & 0 & 0 & 0 & 1 & 0
\end{bmatrix}
\tag{4.44}
$$

First, consider the generic p.c.c. indices, $\delta_g = [3,3]$ and the corresponding similarity transformation matrix,

$$
\mathcal{C}_g = \begin{bmatrix} [B]^1 & A[B]^1 & A^2[B]^1 & [B]^2 & A[B]^1 & A^2[B]^2 \end{bmatrix}
\tag{4.45}
$$

$$
= \begin{bmatrix}
0 & \frac{1}{m_1} & -\frac{d_1}{m_1^2} & 0 & 0 & 0 \\
\frac{1}{m_1} & -\frac{d_1}{m_1^2} & \frac{\frac{d_1^2}{m_1^2}-\frac{k_1}{m_1}+\frac{d_1^2}{m_1 m_2}}{m_1} & 0 & 0 & 0 \\
0 & 0 & \frac{d_1}{m_1 m_2} & 0 & 0 & 0 \\
0 & \frac{d_1}{m_1 m_2} & -\frac{\frac{d_1^2}{m_2^2}-\frac{k_1}{m_2}+\frac{d_1^2}{m_1 m_2}}{m_1} & 0 & 0 & 0 \\
0 & 0 & 0 & 0 & \frac{1}{m_1+m_2} & -\frac{d_2}{(m_1+m_2)^2} \\
0 & 0 & 0 & \frac{1}{m_1+m_2} & -\frac{d_2}{(m_1+m_2)^2} & -\frac{\frac{k_2}{m_1+m_2}-\frac{d_2^2}{(m_1+m_2)^2}}{m_1+m_2}
\end{bmatrix}
\tag{4.46}
$$

It can be seen that $\mathcal{C}_g$ is rank deficient as the sixth column is spanned by the fourth and fifth column. Therefore, by virtue of Theorem 6, it is concluded that generic indices are not admissible for this system. This is a result of the second-order SISO system being decoupled from the fourth-order system. For this reason, adding a spring or damper to m_2 which connects these independent systems would result in the generic indices being admissible as shown in the next paragraph.

Alternatively, specific indices can be used to describe the proportionally damped mechanical system. Consider the specific indices $\delta_s = [4,2]$ and the corresponding similarity transformation

matrix

$$\mathcal{C}_s = \begin{bmatrix} [B]^1 & A[B]^1 & A^2[B]^1 & A^3[B]^1 & [B]^2 & A[B]^2 \end{bmatrix} \tag{4.47}$$

$$= \begin{bmatrix} 0 & \frac{1}{m_1} & -\frac{d_1}{m_1^2} & \frac{d_1^2 m_1 + d_1^2 m_2 - k_1 m_1 m_2}{m_1^3 m_2} & 0 & 0 \\ \frac{1}{m_1} & -\frac{d_1}{m_1^2} & \frac{d_1^2 m_1 + d_1^2 m_2 - k_1 m_1 m_2}{m_1^3 m_2} & -\frac{d_1(m_1+m_2)(d_1^2 m_1 + d_1^2 m_2 - 2 k_1 m_1 m_2)}{m_1^4 m_2^2} & 0 & 0 \\ 0 & 0 & \frac{d_1}{m_1 m_2} & -\frac{d_1^2 m_1 + d_1^2 m_2 - k_1 m_1 m_2}{m_1^2 m_2^2} & 0 & 0 \\ 0 & \frac{d_1}{m_1 m_2} & -\frac{d_1^2 m_1 + d_1^2 m_2 - k_1 m_1 m_2}{m_1^2 m_2^2} & \frac{d_1(m_1+m_2)(d_1^2 m_1 + d_1^2 m_2 - 2 k_1 m_1 m_2)}{m_1^3 m_2^3} & 0 & 0 \\ 0 & 0 & 0 & 0 & 0 & \frac{1}{m_1+m_2} \\ 0 & 0 & 0 & 0 & \frac{1}{m_1+m_2} & -\frac{d_2}{(m_1+m_2)^2} \end{bmatrix} \tag{4.48}$$

The similarity transformation matrix has now full matrix rank. This is a result of the p.c.c. indices being equal to the McMillan degrees of the individual SISO system, see Theorem 7. Therefore, for the proportionally damped system considered in this example, specific indices are admissible.

General Damping

In this paragraph, the damping constant d_2 is set to an arbitrary positive value. Therefore, the horizontal movement is no longer decoupled from the vertical movement which makes the system inherently multivariable. Next, consider the following state-space representation of the mechanical system as function of the angle θ,

$$A = \begin{bmatrix} 0 & 1 & 0 & 0 & 0 & 0 \\ -\frac{k_1}{m_1} & -\frac{d_1}{m_1} - \frac{d_4 \cos(\theta)^2}{m_1} & \frac{k_1}{m_1} & \frac{d_1}{m_1} & 0 & -\frac{d_4 \cos(\theta)\sin(\theta)}{m_2} \\ 0 & 0 & 0 & 1 & 0 & 0 \\ \frac{k_1}{m_2} & \frac{d_1}{m_2} & -\frac{k_1}{m_2} & -\frac{d_1}{m_2} & 0 & 0 \\ 0 & 0 & 0 & 0 & 0 & 1 \\ 0 & -\frac{d_4 \cos(\theta)\sin(\theta)}{m_1+m_2} & 0 & 0 & -\frac{k_2}{m_1+m_2} & -\frac{d_2}{m_1+m_2} - \frac{d_4 \sin(\theta)^2}{m_1+m_2} \end{bmatrix} \tag{4.49}$$

$$B = \begin{bmatrix} 0 & 0 \\ \frac{1}{m_1} & 0 \\ 0 & 0 \\ 0 & 0 \\ 0 & 0 \\ 0 & \frac{1}{m_1+m_2} \end{bmatrix} \tag{4.50}$$

$$C = \begin{bmatrix} 0 & 0 & 0 & 0 & \frac{d_1}{m_1 m_2} & -\frac{d_1^2 m_1 + d_1^2 m_2 - k_1 m_1 m_2 + d_1 d_4 m_2 \cos(\theta)^2}{m_1^2 m_2^2} \\ 0 & 0 & 0 & \frac{1}{m_1+m_2} & -\frac{d_4 \sin(2\theta)}{2 m_1 (m_1+m_2)} & \frac{d_4 \cos(\theta)\sin(\theta)(-d_4 m_2 \sin(\theta)^2 + d_1 m_1 + d_1 m_2 + d_2 m_1 + d_4 m_1 + d_4 m_2)}{m_1^2 (m_1+m_2)^2} \end{bmatrix} \tag{4.51}$$

First, consider the generic p.c.c. indices $\delta_g = [3,3]$ and the corresponding similarity transformation matrix,

$$\mathcal{C}_g = \begin{bmatrix} [B]^1 & A[B]^1 & A^2[B]^1 & [B]^2 & A[B]^1 & A^2[B]^2 \end{bmatrix} \tag{4.52}$$

$$= \begin{bmatrix} 1 & 0 & 0 & 0 & 0 & 0 \\ 0 & 1 & 0 & 0 & 0 & -\frac{k_2}{m_1+m_2} \\ 0 & 0 & 1 & 0 & 0 & -\frac{d_3 k_1 m_2 \cos(\theta)\sin(\theta)}{(m_1+m_2)(k_1 m_2 - d_1 d_3 \cos(\theta)^2)} \\ 0 & 0 & 0 & 1 & 0 & -\frac{d_1 d_2 d_3 - 2 d_2 k_1 m_2 - d_3 k_1 m_2 + d_1 d_2 d_3 \cos(2\theta) + d_3 k_1 m_2 \cos(2\theta)}{(m_1+m_2)(d_1 d_3 - 2 k_1 m_2 + d_1 d_3 \cos(2\theta))} \\ 0 & 0 & 0 & 0 & 1 & -\frac{d_1 d_3 \cos(\theta)\sin(\theta)}{k_1 m_2 - d_1 d_3 \cos(\theta)^2} \\ 0 & 0 & 0 & 0 & 0 & -\frac{d_3 m_1 m_2 \cos(\theta)\sin(\theta)}{(m_1+m_2)(k_1 m_2 - d_1 d_3 \cos(\theta)^2)} \end{bmatrix} \tag{4.53}$$

Clearly, $\mathcal{C}_g$ has full matrix rank as long as the damper corresponding to d_2 is not horizontal or vertical, i.e.

$$\theta \neq k\frac{\pi}{2}, \ k \in \mathbb{Z}. \tag{4.54}$$

If the above condition is satisfied, the generic indices are admissible for this system. The key reason for the generic indices being admissible is that the second order system G_2 is now coupled to the fourth order system G_1 through a diagonal damper d_2 which is connected to the mass m_2.

Alternatively, specific indices can be used to describe the proportionally damped mechanical system. Consider the specific indices $\delta_s = [4, 2]$ and the corresponding similarity transformation matrix,

$$\mathcal{C}_s = \begin{bmatrix} [B]^1 & A[B]^1 & A^2[B]^1 & A^3[B]^1 & [B]^2 & A[B]^2 \end{bmatrix} \tag{4.55}$$

$$= \begin{bmatrix} 1 & 0 & 0 & 0 & 0 & 0 \\ 0 & 1 & 0 & 0 & 0 & 0 \\ 0 & 0 & 1 & 0 & 0 & 0 \\ 0 & 0 & 0 & 1 & 0 & 0 \\ 0 & 0 & 0 & 0 & 1 & 0 \\ 0 & 0 & 0 & 0 & 0 & 1 \end{bmatrix} \tag{4.56}$$

The similarity transformation matrix has now full matrix rank. Therefore, for both the proportionally and generally damped system considered in this example, specific indices are admissible.

On the other hand, examples can be constructed in which generic indices are preferred over specific indices. As a result, selecting either generic indices or specific indices cannot be recommended. Instead, the choice in indices should be made based on the considered mechanical system and the corresponding requirements on the model.

4.4 Overview

In this chapter, an RMFD parametrization is developed based on p.c.c. indices. The parametrization enables a tractable numerical identification through SK and GN iterations as will be shown in Chapter 5. In addition, constraints are proposed to enforce rigid-body modes and a relative degree larger than 1. To enforce rigid-body modes, a trivial parameter constraint is provided. A relative degree is enforced by selecting generic indices or specific indices.

The parametrization enables the model order selection procedure since (i) it that allows an arbitrary model order and (ii) for a given order of the nominal model, the parametrization using generic and specific indices describes a rich class of mechanical systems. In view of (ii), it is shown that a system described using generic indices, is generically equivalent to a mechanical system $\phi \in \Phi_{gd}$. Although this is a very appealing property, it does not mean that all mechanical systems $\phi \in \Phi_{gd}$ can be described by a system described by means of generic indices μ_g. It is shown by Theorem 7, that the choice between selecting generic indices and specific indices should be made case-specific. This is also motivated by means of a mechanical example in the third section.

Chapter 5

Numerical Synthesis of the Robust-Control-Relevant Model Set

The aim of this chapter is to develop a numerical algorithm to identify the robust-control-relevant model set. To construct the model set, a nominal model must be identified first. A second step in the construction of the model set is the computation of the size of the model uncertainty. Thereafter, based on the nominal model and the model uncertainty, the robust-control-relevant model set is constructed.

In the first section, the coprime identification procedure developed in Chapter 3 is reformulated to a frequency domain identification procedure. Next, based on the MFD parametrization proposed in Chapter 4, a numerical procedure to estimate the parametric nominal model is developed. In the last section, a numerical procedure to compute the size of the model uncertainty is investigated.

5.1   Frequency Domain Coprime Factor Identification

In this section, a first step to arriving at a tractable numerical procedure to estimate robust-control-relevant coprime factors is taken. Therefore, $\hat{P}$ is parameterized as RMFD, $\hat{P} = B(\theta)A^{-1}(\theta)$ as defined in Chapter 4. The RMFD parametrization results in the following robust-control-relevant coprime factors,

$$\begin{bmatrix} \hat{N}(\theta) \\ \hat{D}(\theta) \end{bmatrix} = \begin{bmatrix} B(\theta) \\ A(\theta) \end{bmatrix} \left(\tilde{D}_e A(\theta) + \tilde{N}_{e,2} V_2^{-1} B(\theta) \right)^{-1}. \tag{5.1}$$

The coprime factors of the true plant P_o are not explicitly known. However, as the true system P_o is stabilized by the experimental controller C^{exp}, it is possible to determine an Frequency Response Function (FRF) of the true system. Based on an FRF of the true system, the coprime factors of the true system P_o are estimated,

$$\begin{bmatrix} \tilde{N}_o(\xi_k) \\ \tilde{D}_o(\xi_k) \end{bmatrix} = \tilde{T}(P_o, C^{exp})(\xi_k) V \tilde{N}_e^*(\xi_k). \tag{5.2}$$

Where $\xi_k = j\omega_k$, where ω_k denotes the k-th frequency. Next, the identification criterion proposed in Theorem 1 is reformulated using the frequency domain definition of the $\mathcal{H}_\infty$-norm,

$$\min_\theta \max_{\omega_k \in \Omega} \bar{\sigma} \left(W \left(\begin{bmatrix} N_o(\xi_k) \\ D_o(\xi_k) \end{bmatrix} - \begin{bmatrix} \hat{N}(\xi_k, \theta) \\ \hat{D}(\xi_k, \theta) \end{bmatrix} \right) \right). \tag{5.3}$$

To determine the optimal parameter vector $\hat{\theta}$, a numerical solver is developed. The numerical procedure is explained in the next section.

5.2 Numerical Solver

In this section, a numerical procedure is developed to reliably identify the robust-control-relevant coprime factors.

Observe that the identification criterion in Eq. (5.3) employs the ℓ_∞-norm, which means that the optimization problem is not smooth. This means that gradient-based techniques are not applicable. Secondly, the parameter vector appears nonlinearly in the parameters. As a result, the problem is non-convex. Therefore, the optimization is split into two parts: i) approximating the ℓ_∞-norm by the ℓ_2-norm. ii) Solving the nonlinear least-squares problem. In Figure 5.1, an overview of the algorithm is depicted. It can be seen that Lawson's algorithm is used to approximate the ℓ_∞-norm and approximates it by a linear least-squares problem. Thereafter, the resulting nonlinear least-squares problem is solved for the parameter vector θ using a two-stage solver. The first stage consists of SK-iterations to provide an estimate of the optimal parameter vector $\hat{\theta}$. In the second stage, the estimate is refined by GN iterations to approximate the optimal parameter vector $\hat{\theta}$. Using the updated θ, a new Lawson-weight is computed and the algorithm repeats itself until convergence.
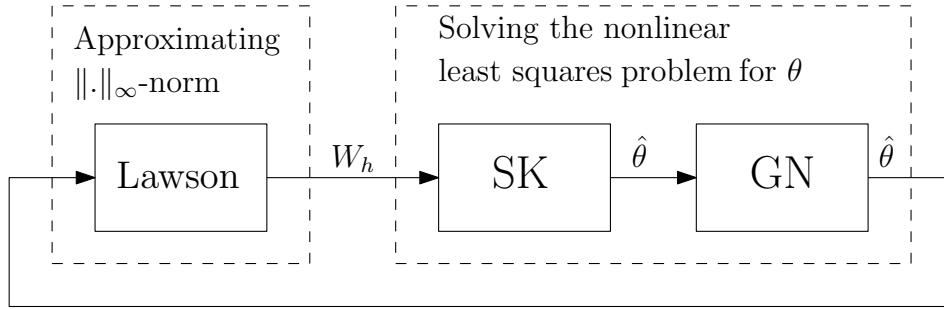

Figure 5.1 Schematic overview of the algorithm used to find the robust-control-relevant nominal model.

5.2.1 Lawson Iterations

To arrive at a nonlinear least-squares problem, the ℓ_∞-norm is approximated through ℓ_2-norm by Lawson's algorithm. Consider Lawson's algorithm [11, 48].

Algorithm 1. Given the initial parameter vector $\theta^{<0>}$ and the initial Lawson-weight $w^{<0>}(\xi_k) = \frac{1}{N_w}$, where N_w denotes the number of frequencies in Ω_{id} and $\xi_k = j\omega_k$, where ω_k denotes the k-th frequency. Iterate over the index $<j>$ until convergence,

$$\theta^{<j>} = \arg\min_\theta \sum_{k=1}^{N_w} w^{<j>}(\xi_k) \left\| \epsilon(\xi_k, \theta) \right\|_F^2. \tag{5.4}$$

Where the weight is defined as,

$$w^{<j>}(\xi_k) = \frac{\bar{\sigma}\left(\epsilon(\xi_k, \theta^{<j>})\right) w^{<j-1>}(\xi_k)}{\sum_{k=1}^{N_\omega} \left(\bar{\sigma}\left(\epsilon(\xi_k, \theta^{<j>})\right) w^{<j-1>}(\xi_k)\right)}. \tag{5.5}$$

Lawson's algorithm essentially approximates the ℓ_∞-norm by the ℓ_2-norm with a weighting that penalizes those frequency-bins with a high contribution in the ℓ_2-norm. Convergence of Lawson's algorithm is not guaranteed, however, numerical experience indicates that this algorithm works well in practice [42]. Next, using the Lawson weighting, Eq. (5.3) is reformulated to,

$$\sum_{k=1}^{N_\omega} \left\| W_h^{<j>}(\xi_k) \circ \left(W\left(\begin{bmatrix} N_o(\xi_k) \\ D_o(\xi_k) \end{bmatrix} - \begin{bmatrix} \hat{N}(\xi_k, \theta) \\ \hat{D}(\xi_k, \theta) \end{bmatrix} \right) \right) \right\|_F^2. \tag{5.6}$$

Herein, $\circ$ denotes the Hadamard product, and $W_h^{<j>} \in \mathbb{R}^{(n_u + n_y) \times 2n_u}$ denotes the Hadamard-Weighting function. The elements of $W_h^{<j>}$ are equal to $\sqrt{w^{<j>}(\xi_k)}$. The resulting optimization problem employs the Frobenius-norm. As a result, the Lawson weighting approximate the ℓ_∞-norm is by a ℓ_2-type norm. In the next subsection, the resulting nonlinear least squares problem is solved.

5.2.2 Nonlinear Least Squares Solver

In the previous section, Lawson's algorithm is employed to approximate the ℓ_∞-norm by the ℓ_2-type norm. This means that a nonlinear least-squares problem is obtained. In this section, a numerical method is proposed to solve Eq. (5.6). Therefore, Eq. (5.6) is reformulated, in the next theorem.

Theorem 8. Given the optimization problem Eq. (5.6), then the optimization problem can be written as

$$\mathcal{V}(\theta) = \sum_{k=1}^{N_\omega} \|\epsilon(\xi_k, \theta)\|_2^2, \tag{5.7}$$

$$= \sum_{k=1}^{N_\omega} \left\| W_{nl}^{<j>}(\xi_k, \theta) \text{vec}\left(\begin{bmatrix} B(\xi_k, \theta) \\ A(\xi_k, \theta) \end{bmatrix} \right) \right\|_2^2, \tag{5.8}$$

where,

$$W_{nl}^{<j>}(\xi_k, \theta) = \text{diag}\left(\text{vec}\left(W_h^{<j>}(\xi_k) \right) \right) \left(\left[\left(\tilde{D}_e A(\theta) + N_{e,2} V_2^{-1} B(\theta) \right)^{-1} \right]^\top \otimes \left[W\left(\begin{bmatrix} N_o \tilde{N}_{e,2} V_2^{-1} & N_o \tilde{D}_e \\ D_0 \tilde{N}_{e,2} V_2^{-1} & D_o \tilde{D}_e \end{bmatrix} - I \right) \right] \right). \tag{5.9}$$

A proof is given in Appendix B.5.

To arrive at a linear least-squares problem, the vectorized numerator- and denominator-matrix of the RMFD structure are written as a linear matrix-vector product in terms of the parameter vector θ in the next theorem.

Theorem 9. Given the RMFD structure of the nominal model $\{A(\theta), B(\theta)\}$. Then, $\text{vec}\begin{bmatrix} \hat{B}(\xi_k, \theta) \\ \hat{A}(\xi_k, \theta) \end{bmatrix}$ may be written as a linear matrix-vector product in terms of the parameter vector θ,

$$\text{vec}\left(\begin{bmatrix} \hat{B}(\xi_k, \theta) \\ \hat{A}(\xi_k, \theta) \end{bmatrix} \right) = b(\xi_k) - \Phi(\xi_k)\theta. \tag{5.10}$$

Herein, $\Phi(\xi_k) = \text{blockdiag}(\Phi_j(\xi_k))$ for $j = 1, ..., n_u$, where $\Phi_j(\xi_k)$ is defined as

$$\Phi_j = \left[\begin{array}{ccc|ccc} & & & F(\nu_j) & & O \\ & O & & & \ddots & \\ & & & O & & F(\nu_j) \\ \hline F(\mu_1) & & O & & & \\ & \ddots & & & O & \\ O & & F(\mu_{n_u}) & & & \end{array} \right] \in \mathbb{C}^{(n_u+n_y)\times(n_x+n_y\nu_j)}. \tag{5.11}$$

Where,

$$F(\kappa) = \begin{bmatrix} 1 & \xi_k & \cdots & \xi_k^{\kappa-1} \end{bmatrix} \in \mathbb{C}^{\kappa\times 1} \tag{5.12}$$

and

$$[b]_i = \left[\begin{array}{c} 0 \\ \vdots \\ 0 \\ \hline \delta_{i1}\xi_k^{\mu_1} \\ \vdots \\ \delta_{in_u}\xi_k^{\mu_{n_u}} \end{array} \right] \in \mathbb{C}^{(n_u+n_y)\times 1} \tag{5.13}$$

A proof is given in Appendix B.6.

In the following paragraphs, a two-stage numerical solver is proposed. First, a nonlinear least squares problem is formulated on the basis of SK iterations. Although this algorithm does not necessarily converge to a global minimum, in practice it is often close to it [67]. In the second paragraph, the second solver stage is explained, GN iterations.

Sanathanan-Koerner Iterations

In this section, the SK algorithm for the identification of the control-relevant-coprime factors is derived. To arrive at the algorithm, observe that for a parameter vector θ to be a minimum to Eq. (5.7), it should be a stationary point. Therefore, the following condition should be satisfied,

$$\left(\frac{\partial \mathcal{V}}{\partial \theta^\top}\right)^H = \sum_{k=1}^{N_\omega} 2\,\text{Re}\left\{\left(W_{nl}^{<j>}(\xi_k, \theta)\Phi(\xi_k)\right)^H \left(b(\xi_k) - \Phi(\xi_k)\theta\right)\right\} = 0. \tag{5.14}$$

To arrive at the nonlinear least-squares problem, the summation is omitted by stacking over the frequency grid,

$$[X_s]_k = W_{nl}^{<j>}(\xi_k, \theta)\Phi(\xi_k), \quad \text{for } k = 1, ..., N_\omega, \tag{5.15}$$

$$[Z_s]_k = W_{nl}^{<j>}(\xi_k, \theta)b(\xi_k), \quad \text{for } k = 1, ..., N_\omega. \tag{5.16}$$

Next, using the matrices X_s and Z_s, a matrix-vector product is derived,

$$\text{Re}\left(X_s^H(Z_s - X_s\theta)\right) = 0. \tag{5.17}$$

The Re-operator is omitted by incorporating it within the following matrices,

$$X = \begin{bmatrix} \text{Re}(X_s) \\ \text{Im}(X_s) \end{bmatrix} \qquad\qquad Z = \begin{bmatrix} \text{Re}(Z_s) \\ \text{Im}(Z_s) \end{bmatrix}. \tag{5.18}$$

This results in the following matrix-vector product,

$$\left(X^H (Z - X\theta) \right) = 0, \tag{5.19}$$

To solve Eq. (5.19) for the parameter vector θ, observe that also the matrices X and Z depend on the parameter vector θ. A key aspect of the SK algorithm is to iteratively solve Eq. (5.19) by approximating the matrices X and Z based on the previously calculated θ [49]. Therefore, given an initial estimate of the parameter vector $\theta^{<0>}$, the matrices X and Z are constructed based on $\theta^{<0>}$. Then, a refined parameter vector is computed by solving Eq. (5.19) for $\theta^{<1>}$. By continuing this procedure over the index i, a refined solution can be found. This procedure is formally defined as follows.

Algorithm 2. SK-iterations.

1. Given the j-th Lawson weight according to Eq. (5.5), the initial estimate of the parameter vector θ and the matrices Φ and b according to Theorem 9.

2. Construct the matrices X and Z based on the i-th parameter vector, $\theta^{<i>}$.

3. Solve Eq. (5.19) for the refined solution $\theta^{<i+1>}$.

4. Continue iterating over the index i until convergence or the maximum number of SK iterations is reached.

The SK-algorithm need not converge, however, in practice, the SK algorithm has shown to provide solutions of the parameter vector θ close to the global minimum [67]. Therefore, SK iterations are suitable for providing an initial estimate for GN iterations [66].

Gauss-Newton Iterations

In the previous paragraph, SK iterations are performed to provide a coarse estimate of the global minimum. To refine the solution, the cost function is locally approximated, resulting in a quadratic cost function. The quadratic cost function is solved by considering a gradient-based optimization scheme. This scheme may lead to convergence to the global minimum. In this research, GN iterations are considered [6].

Given a perturbation $\delta\theta$ around a fixed parameter vector $\theta^{<f>}$. Next, consider the stationary condition applied to Eq. (5.7) evaluated at $\theta^{<f>} + \delta\theta$,

$$\left(\frac{\partial \mathcal{V}(\theta^{<f>} + \delta\theta)}{\partial \delta\theta^\top} \right)^H = \sum_{k=1}^{N} -2\operatorname{Re}\left\{ \left(\frac{\partial \epsilon(\xi_k, \theta^{<f>} + \delta\theta)}{\partial \delta\theta^\top} \right)^H \epsilon(\xi_k, \theta^{<f>} + \delta\theta) \right\}, \tag{5.20}$$

$$= 0. \tag{5.21}$$

Now, consider a first order Taylor expansion on the weighted error $\epsilon(\xi_k, \theta + \delta\theta)$,

$$\epsilon(\xi_k, \theta^{<f>} + \delta\theta) \approx \epsilon(\xi_k, \theta^{<f>}) - W_{nl}^{<j>}(\xi_k, \theta^{<f>})\Phi(\xi_k)\delta\theta. \tag{5.22}$$

Combining Eq. (5.20) and (5.22) gives,

$$\left(\frac{\partial \mathcal{V}(\theta^{<f>} + \delta\theta)}{\partial \delta\theta^\top} \right)^H = \sum_{k=1}^{N} 2\operatorname{Re}\left\{ \left(W_{nl}^{<j>}(\xi_k, \theta^{<f>})\Phi(\xi_k) \right)^H \left(\epsilon(\xi_k, \theta^{<f>}) - W_{nl}^{<j>}(\xi_k, \theta^{<f>})\Phi(\xi_k)\delta\theta \right) \right\}, \tag{5.23}$$

$$= 0. \tag{5.24}$$

To arrive at the nonlinear least squares problem, the summation is omitted by stacking over the frequency grid,

$$[X_s]_k = W_{nl}^{<j>}(\xi_k, \theta^{<f>})\Phi(\xi_k), \quad \text{for } k = 1, ..., N_\omega, \tag{5.25}$$

$$[Z_s]_k = \epsilon(\xi_k, \theta^{<f>}), \quad \text{for } k = 1, ..., N_\omega. \tag{5.26}$$

Next, using the matrices X_s and Z_s, a matrix vector product is derived,

$$\text{Re}\left(X_s^H(Z_s - X_s\delta\theta)\right) = 0. \tag{5.27}$$

The Re-operator is omitted by incorporating it within the following matrices

$$X = \begin{bmatrix} \text{Re}(X_s) \\ \text{Im}(X_s) \end{bmatrix} \qquad\qquad Z = \begin{bmatrix} \text{Re}(Z_s) \\ \text{Re}(Z_s) \end{bmatrix}. \tag{5.28}$$

Using these matrices, Eq. (5.27) is rewritten to

$$\left(\tilde{X}_{GN}^H(\tilde{Z}_{GN} - \tilde{X}_{GN}\delta\theta)\right) = 0. \tag{5.29}$$

The linear system of equations in Eq. (5.29) can be solved for the perturbation $\delta\theta$. The key aspect of the GN algorithm is to compute an updated parameter vector by taking $\theta^{<f+1>} = \theta^{<f>} + \delta\theta$ and to iterate over the index $< f >$. Although this algorithm may not converge to the local minimum, in practice, it has shown to provide appropriate solutions. Now consider the formal algorithm of GN iterations.

Algorithm 3. GN-iterations.

1. Given the j-th Lawson weight according to Eq. (5.5), the initial estimate of the parameter vector $\theta^{<0>} = \theta^{<i>}$ and the matrices Φ and b according to Theorem 9.

2. Construct the matrices X and Z based on the f-th parameter vector, $\theta^{<f>}$.

3. Solve Eq. (5.29) for the perturbation $\delta\theta$, and compute the updated parameter vector $\theta^{<f+1>} = \theta^{<f>} + \delta\theta$.

4. Continue iterating over the index $< f >$ until convergence or the maximum number of GN iterations is reached.

5.2.3   Iteration Scheme

In the previous paragraphs, the numerical steps to identify the robust-control-relevant nominal model are discussed. In this subsection, a short overview is given of the numerical algorithm to identify the robust-control-relevant nominal model. Consider the following algorithm.

Algorithm 4. Numerical algorithm for robust-control-relevant identification of the nominal model.

1. Lawson. Compute the j-th Lawson-weight according to Eq. (5.5).

2. Sanathanan and Koerner (SK). Solve the nonlinear least-squares problem according to Algorithm 2 by iterating over the index $< i >$ until convergence or if the maximum number of iterations is reached.

3. Gauss-Newton (GN). Solve the nonlinear least-squares problem according to Algorithm 3 by iterating over the index $<f>$ until convergence or if the maximum number of iterations is reached.

4. If the maximum number of Lawson-iterations is reached or if convergence is achieved, stop iterations. Else, continue Lawson-iterations over $<j>$ by $j \leftarrow j + 1$.

5.3 Robust-Control-Relevant Model Set

The robust-control-relevant is constructed based on a nominal model, and the size of the model uncertainty. In the previous sections, an algorithm to compute the nominal model is developed. In this section, a method to determine the size of the model uncertainty is investigated. To arrive at this method, consider Figure 5.2. In this figure, a block diagram of the dual-Youla-Kučera uncertainty structure is depicted.
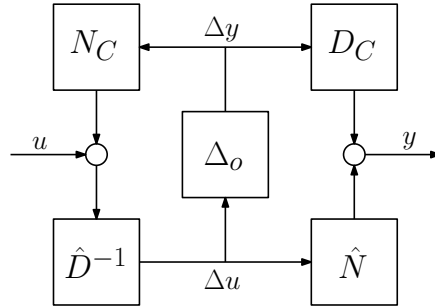
Figure 5.2 Block diagram of the dual Youla Kučera model structure for the true system P_o.

A key aspect of the dual-Youla-Kučera model structure is that it parameterizes all systems stabilized by the experimental controller C^{exp}. As a result, there exists a perturbation Δ_o such that the dual-Youla-Kučera model structure represents the true model P_o [45]. This is formally written as,

$$\exists \Delta_o \in \mathcal{RH}_\infty, \text{ s.t. } \mathcal{F}_u(\hat{H}, \Delta_o) = P_o. \tag{5.30}$$

To find a Δ_o, first, recall that the model structure is given by,

$$P_o = \left(\hat{N} + D_C\Delta_o\right)\left(\hat{D} - N_C\Delta_o\right)^{-1}. \tag{5.31}$$

The Δ_o that satisfies Eq. (5.30), is found by rewriting Eq. (5.31) to,

$$\Delta_o = D_C^{-1}\left(I + P_oC\right)^{-1}\left(P_o - \hat{P}\right)\hat{D}. \tag{5.32}$$

The smallest size of the model uncertainty, γ, such that $P_o \in \mathcal{P}^{RCR}$ is therefore given by,

$$\gamma = \|\Delta_o\|_\infty. \tag{5.33}$$

However, the true system P_o and, as a consequence, the true uncertainty Δ_o are not known explicitly. To approximate the true uncertainty Δ_o, an FRF of the true system is used. Next, using the approximation of the true system, the size of the model uncertainty may be computed by considering the frequency domain definition of Eq. (5.33),

$$\gamma = \max_\omega \Delta_o(j\omega), \quad \omega \in \Omega_{id}. \tag{5.34}$$

Where Ω_{id} denotes the set of frequencies at which the FRF of the true system is performed.

Chapter 6

Controller Synthesis

The aim of this chapter is to investigate the synthesis of the robust controller based on the robust-control-relevant model set. A key element of a robust controller is that it is optimal with respect the performance criterion. For this reason, specifying the weighting filters is crucial. The weighting filter design is investigated in the first section. Thereafter, the robust controller synthesis algorithm considered in this research is discussed.

6.1 Weighting Filter Design

In this section, the weighting filter design is investigated. To come up with a relevant weighting filter design, first, the controller objectives are discussed. Second, the controller objectives are translated into the weighting filter design.

6.1.1 Control Objectives

To synthesis a robust controller, it is essential to formulate the control objective. For the formulation of the control objectives, the closed-loop bandwidth is a crucial concept. Consider the definition of the closed-loop bandwidth.

Definition 20. Closed-loop bandwidth. Given the singular values of the open-loop, $q_i = \sigma_i(PC)$. Then, the i-th closed-loop bandwidth is defined as the smallest frequency $f_{bw,i}$ for which the following equality holds,

$$q_i(2\pi f_{bw,i}) = 1. \tag{6.1}$$

Often, motion systems are decoupled such that the plant P is approximately diagonal. Therefore, diagonal controllers are used. As a result, the i-th bandwidth $f_{bw,i}$ is defined as the smallest frequency at which the i-th diagonal component equals one, i.e. $|P_{ii}(2\pi f_{bw,i})C_{ii}(2\pi f_{bw,i})| = 1$.

For many motion systems, it is desired to perform tracking with high accuracy. Regarding the tracking performance, the following relation is crucial,

$$\bar{\sigma}(S_o) \simeq \frac{1}{\underline{\sigma}(P_oC)}, \quad S_o = (I + P_oC)^{-1}, \tag{6.2}$$

when $\underline{\sigma}(P_oC) \gg 1$. Next, observe that in terms of tracking performance, it is desired to have a small output sensitivity. This is achieved by having a high loop gain, i.e. $\underline{\sigma}(PC) \gg 1$. This motivates the choice of a high gain for low frequencies and a high bandwidth.

On the other hand, for mechanical systems, it is desired to have sufficient sensor noise suppression at high frequencies. Related to the noise suppression, observe that the following relation holds for the complementary sensitivity function,

$$\bar{\sigma}(T_o) \simeq \bar{\sigma}(P_oC), \quad T_o = P_oC(I + P_oC)^{-1}, \tag{6.3}$$

if $\bar{\sigma}(P_oC) \gg 1$. Next, in terms of noise suppression, observe that $\bar{\sigma}(T_o)$ should be made small. This motivates the use of roll-off to keep $\bar{\sigma}(P_oC)$ small at high frequencies.

6.1.2 Weighting Filter Design

The synthesis of a robust controller requires the design of the closed-loop weighting filters W and V, see Definition 1. In this research, loop-shaping-based weighting filters are used to specify the robust control objectives. This approach is based on the approach proposed in [37, 64]. The key reason for choosing open-loop weighting filters is that they allow integral action and roll-off. Secondly, since the design is loop-shaping based the design intuitive.

The approach consists of the weighting filters W_1 and W_2. Using these weighting filters, the desired loop-shape is constructed,

$$P_s = W_2 P_o W_1. \tag{6.4}$$

It must be noted that the loop-shaping-based approach weighting filter design approach originally used the nominal model for the weighting filter design. However, for the joint identification and robust controller synthesis framework developed in this research, this is not possible. Instead, a FRF of the true system is used for the weighting filter design. The loop-shaping based weighting filters are related to the closed-loop weighting filters as follows,

$$W = \begin{bmatrix} W_2 & 0 \\ 0 & W_1^{-1} \end{bmatrix}, \qquad\qquad V = \begin{bmatrix} W_2^{-1} & 0 \\ 0 & W_1 \end{bmatrix}. \tag{6.5}$$

In view of Eq. (6.2), the desired loop shape is made large at low frequencies. This is achieved by enforcing integral action through the weighting filter W_1. On the other hand, in view of Eq. (6.3), it is desired to shape P_s such that at high frequencies, the magnitude of the open-loop is small. Therefore, controller roll-off is enforced by adding roll-off to the weighting filter W_2. Although the robust controller synthesis only constructs stabilizing controllers, the shaped plant should be designed such that it is not unnecessarily hard to construct a stabilizing controller. Therefore, controller roll-off is enforced sufficiently far away from the desired bandwidth. In addition, a '+1' slope can be enforced around the desired bandwidth if large phase margins are desired. The desired bandwidth is enforced by adjusting the gain of W_1 or W_2. In this research, the gain is equally distributed about the weighting filter for numerical conditioning, for details see [58].

6.1.3 Procedure

A key aspect of the open-loop weighting filters considered in this research is that the weighting filters are absorbed in the closed-loop during the robust controller synthesis. This is shown in the block diagram in Figure 6.1.
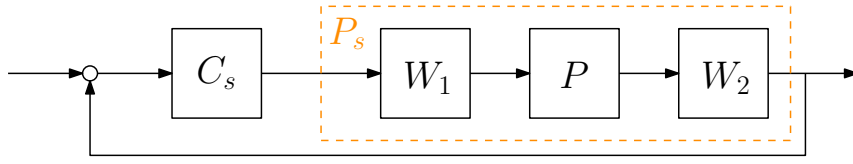
Figure 6.1 Block diagram of the closed-loop system with loop-shaping-based weighting filters.

In Figure 6.1, C_s denotes the shaped controller which is related to the true controller as follows,

$$C = W_2 C_s W_1. \tag{6.6}$$

As the loop-shaping-based weighting filters are absorbed in the closed-loop, the cost function Eq. (2.2) is reformulated in the next definition.

Definition 21. Cost function for open-loop weighting filters. Given the loop-shaping-based weighting filters, Eq. (6.5), then Eq. (2.2) is equal to,

$$\mathcal{J} = \|T(P_s, C_s)\|_\infty. \tag{6.7}$$

Where P_s is in accordance with Eq. (6.4) and C_s is defined as Eq. (6.6).

The controller synthesis for the loop-shaping-based weighting filters is formulated as

$$C_s^{RP} = \arg \min_{C_s} \left(\mathcal{J}_{WC} \left(\mathcal{P}^{RCR}(\hat{P}_s, C_s^{exp}), C_s \right) \right). \tag{6.8}$$

6.2 Controller Synthesis

In this section, the synthesis of the optimal controller is discussed. The synthesis procedure is also valid for open-loop and closed-loop weighting filters. Since closed-loop weighting filters encompass open-loop weighting filters, the procedure is derived for closed-loop weighting filters.

Given the general formulation for the robust controller synthesis,

$$C^{RP} = \arg \min_{C} \left(\mathcal{J}_{WC} \left(\mathcal{P}^{RCR}, C \right) \right). \tag{6.9}$$

The computation of the optimal controller is split into two parts. The first part encompasses the computation of $\mathcal{J}_{WC} \left(\mathcal{P}^{RCR}, C \right)$ for an arbitrary stabilizing controller C. The second part encompasses the minimization in Eq. (6.9). In the first section, the computation of the worst-case performance is investigated. In the second section, the optimization procedure is discussed.

6.2.1 Computation of worst-case performance

To compute $\mathcal{J}_{WC} \left(\mathcal{P}^{RCR}, C \right)$ for an arbitrary stabilizing controller C, observe that $\mathcal{J}_{WC} \left(\mathcal{P}^{RCR}, C \right)$ is equal to,

$$\mathcal{J}_{WC} \left(\mathcal{P}^{RCR}, C \right) = \sup_{\|\Delta_u\|_\infty \leq \gamma} \left\| \mathcal{F}_u \left(\tilde{M}^{RCR}(\mathcal{P}^{RCR}, C), \Delta_u \right) \right\|_\infty. \tag{6.10}$$

Herein, $\tilde{M}^{RCR}(\mathcal{P}^{RCR}, C)$ denotes the weighted closed-loop. To compute the weighted closed-loop, consider the block diagram in Figure 6.2.
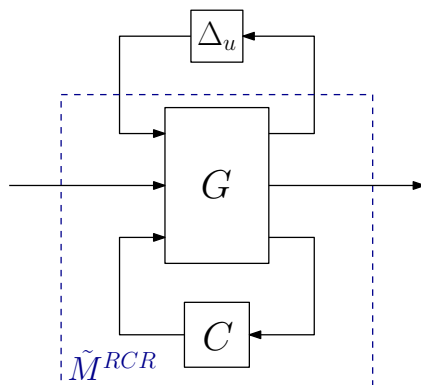
Figure 6.2 Block diagram indicating the $M\Delta$-structure.

In this figure, the weighted closed-loop is defined as the lower LFT of G in combination with the stabilizing controller C,

$$\tilde{M}^{RCR} = \mathcal{F}_l\left(G, C\right). \tag{6.11}$$

Herein, the transfer matrix G is defined as [47],

$$G = \left[\begin{array}{cc|cc|c} \gamma\hat{D}^{-1}N_C & 0 & \gamma\hat{D}^{-1}V_1 & \gamma\hat{D}^{-1} \\ \hline W_y\left(D_C + \hat{P}N_C\right) & 0 & W_y\hat{P}V_1 & W_y\hat{P} \\ 0 & 0 & W_uV_1 & W_u \\ \hline -D_C - \hat{P}N_C & V_2 & -\hat{P}V_1 & -\hat{P} \end{array}\right]. \tag{6.12}$$

For the computation of the worst-case performance, the SSV plays a crucial role. Therefore, the following definition is essential.

Definition 22. Structured Singular Value (SSV). Given a complex transfer matrix M and the perturbation Δ. Then the structured singular value is defined as,

$$\mu_\Delta(M(j\omega) = \left\{\min_\Delta \left\{\bar{\sigma}(\Delta) | \det\left(I - M\Delta\right) = 0\right\}\right\}^{-1}. \tag{6.13}$$

The value of the SSV depends on the structure of the uncertainty block Δ. If Δ is unstructured, the structured singular value is given by $\mu\left(\Delta\right)) = \bar{\sigma}\left(\Delta\right)$. Furthermore, given the peak-μ of $M\Delta$-structure, $\sup_\omega \mu_\Delta(M(j\omega) = \beta$. The peak-value means that the uncertainty block may be increased by a factor $\frac{1}{\beta}$, before instability is reached.

To compute the supremum in Eq. (6.9), consider Figure 6.3. In this figure, a fictitious unstructured performance uncertainty block, Δ_p is placed between the input and output. The maximum allowable magnitude $\|\Delta_p\|$ is directly related to the worst-case performance.
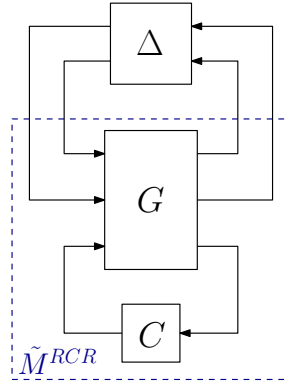
Figure 6.3 Block diagram indicating the $M\Delta$-structure.

Next, the model uncertainty and the fictitious performance block are lumped into a single uncertainty block,

$$\Delta = \begin{bmatrix} \Delta_u & \\ & \Delta_p \end{bmatrix}. \tag{6.14}$$

To compute the maximum allowable magnitude of the fictitious performance block, the SSV is unsuitable, as the magnitude of Δ_u is fixed, while the magnitude of the fictitious performance block is to be optimized. Therefore, consider the definition of the skewed-μ.

Definition 23. Skewed-μ. Given the complex matrix M and the perturbation Δ_u. Then the skewed-μ-value is defined as,

$$\mu_s \left(M(j\omega) \right) = \max_{\|\Delta_u\|_\infty \leq \gamma} \left\{ \|\mathcal{F}_u \left(M(j\omega), \Delta_u \right)\|_\infty \right\}. \tag{6.15}$$

To find μ^s, consider the lumped the perturbation $\Delta = \text{diag} \left(\Delta_u, \Delta_p \right)$. Then, μ_s is the value to results in,

$$\mu_\Delta \left(K_m M \right) = \gamma, \qquad\qquad K_m = \begin{bmatrix} I & 0 \\ 0 & \frac{1}{\mu_s} \end{bmatrix}. \tag{6.16}$$

In this research, a bisection algorithm is used to find μ_s [54].

Next, using the definition of the skewed-μ, the worst-case performance is calculated as,

$$\mathcal{J}_{WC} \left(\mathcal{P}^{RCR}, C \right) = \max_\omega \mu_s \left(\tilde{M}^{RCR}(j\omega) \right), \quad \omega \in \Omega_{wc} \tag{6.17}$$

Herein, Ω_{wc} denotes the set of frequencies at which the skewed-μ analysis is performed.

6.2.2 DK-Iterations

Currently, there does not exist a method to synthesizes a robust controller that minimizes Eq. (6.9) directly. However, to approximate the minimization in Eq. (6.9), DK-iterations may be used. This method combines the synthesis of a $\mathcal{H}_\infty$-controller with the value of the skewed-μ analysis.

The *DK* iterations are based on an upper bound of the SSV, which is defined in the following definition.

Definition 24. Consider the set of matrices $\mathcal{D}$ that commute with the lumped uncertainty block Δ, i.e. $\Delta D = D\Delta$. Then the following bound on the SSV holds [54],

$$\mu(M) \leq \min_{D \in \mathcal{D}} \bar{\sigma}(DMD^{-1}). \tag{6.18}$$

In this research, a skewed-μ optimal controller is synthesized. Therefore, Eq. (6.18) and Eq. (6.16) are combined.

$$\mu(K_m M) \leq \min_{D \in \mathcal{D}} \bar{\sigma}(DK_m MD^{-1}). \tag{6.19}$$

As the lumped perturbation block contains two unstructured perturbation blocks, the bound in Eq. (6.19) is tight [54]. This means, that the structured singular value is determined without conservatism. Next, Eq. (6.19) is used to synthesis the robust controller,

$$C^{RP} = \arg \min_{C} \left(\min_{D} \left\| DK_m M(C)D^{-1} \right\|_{\infty} \right). \tag{6.20}$$

The key idea of DK-iterations is to alternate the minimization of $\left\| DK_m M(C)D^{-1} \right\|_{\infty}$ with respect to the controller C and the matrix D. DK-iterations involves two convex optimization problems. However, the combined problem, the robust controller synthesis, is a non-convex optimization problem. Therefore, the DK-algorithm does not necessarily converge to the optimal robust controller. However, the algorithm works well in practice. Next, consider the DK-algorithm.

Algorithm 5. DK-iterations.

1. Initial conditions. Select an appropriate initial stable and rational transfer function $D(s)$.

2. K-Step. Synthesize a controller $\hat{C}^{RP}$ that minimizes $\left\| DK_m M(C)D^{-1} \right\|_{\infty}$.

3. D-step.

    (a) Compute $D(j\omega)$ that minimizes $DK_m M(\hat{C}^{RP})D^{-1}$ at each frequency $\omega \in \Omega_{DK}$.

    (b) Fit an appropriate stable and minimum phase transfer $D(s)$ to the data obtained in (a).

4. Skewed-μ synthesis. Compute the value of the skewed-μ analysis, $\mu^s(M)$ and construct the matrix K_m. Next, continue to the K-step.

The iterations may be canceled if a sufficient amount of convergence is achieved or if the maximum number of iterations is reached.

Chapter 7

Simulation Example

In this chapter, the joint identification and robust controller synthesis framework with model order selection procedure developed in this research is applied in a simulation example which is representative for many motion systems. First, the mechanical system considered in this case study is discussed. Thereafter, the initial controller and the weighting filter design are explained. Next, the robust-control-relevant identification procedure with optimal model order selection is executed for various bandwidths. Lastly, using the robust-control-relevant model sets with their corresponding optimal model orders, the robust controllers are synthesized in the last section.

7.1 Mechanical System

In this subsection, the mechanical system considered in this chapter is explained. Although the entire framework is valid for MIMO systems, it is applied to a SISO example due to time limitations.

Figure 7.1 depicts the three-mass-spring-damper-system considered in this chapter. Herein, F denotes the actuator force, x_1 denotes the collocated position of the first mass, m_1. The parameter k_i denote the i-th spring constant and d_i denotes the i-th damping constant. It can easily be seen that this system contains one rigid-body mode and two flexible modes.
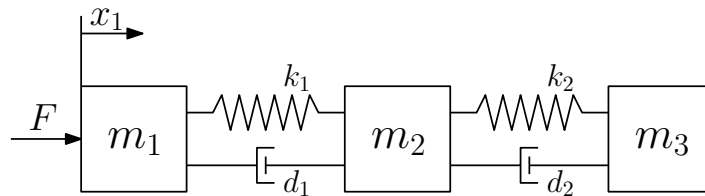
Figure 7.1 Free body diagram of the collocated plant.

The Bode diagram of parameterized system is depicted in Figure 7.2. The system contains two flexible modes, there are two anti-resonances, $f = 8.5$ Hz and $f = 26$ Hz and two resonances at $f = 12$ Hz and $f = 28.4$ Hz. In this chapter, the true system P_o is explicitly known, however, it is emphasized that joint identification and robust controller synthesis framework developed in this research only requires an FRF estimate of the true system $P_o(j\omega)$.
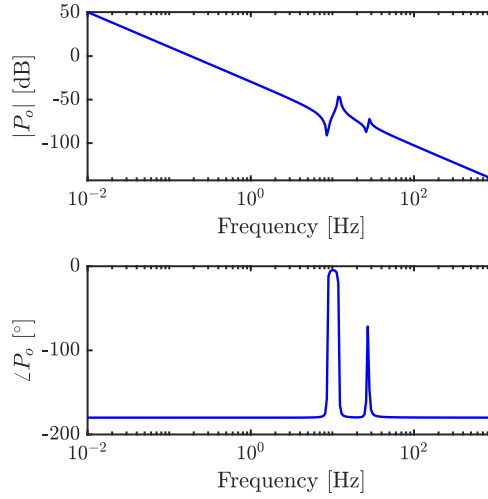
Figure 7.2 Bode diagram of the true plant P_o.

7.2 Order Selection Procedure

Recall from Eq. (3.24) that for the selection of model order, the following cost function is considered,

$$\mathcal{W}(n_x) = \gamma(n_x) + \tilde{\phi} n_x. \tag{7.1}$$

Next, the optimal model order n_x^* is computed according to,

$$n_x^* = \arg\min_{n_x} \mathcal{W}(n_x). \tag{7.2}$$

To arrive at the selection of the tuning parameter $\tilde{\phi}$, let $n_{x,i}$ be the i-th model order at which the order selection procedure is evaluated. Then, the corresponding uncertainty magnitude is $\gamma(n_{x,i})$. Next, the worst-case performance with respect to the i-th iteration of the order selection procedure is approximated as $\mathcal{J}(P_o, C^{exp}) + 2\gamma(n_{x,i})$ by considering the upper bound of the worst-case performance proposed in Theorem 2. Now, assume that at least $0 \leq \alpha \leq 1$ performance increase is required before it is allowed to increase the model order from $n_{x,0}$ to $n_{x,1}$. In other words, increasing the model order is allowed if the following inequality is satisfied,

$$(1 - \alpha)(J(P_o, C^{exp}) + 2\gamma(n_{x,0})) \geq J(P_o, C^{exp}) + 2\gamma(n_{x,1})). \tag{7.3}$$

The resulting tuning parameter ϕ is defined as

$$\tilde{\phi} = \frac{\alpha(J(P_o, C^{exp}) + 2\gamma(n_{x,0}))}{n_{x,1} - n_{x,0}}. \tag{7.4}$$

In this example, the parameter is defined as $\alpha = 0.05$. Hence, at least 5% performance increase is required before it is allowed to enlarge the initial order from $n_{x,0}$ to $n_{x,1}$. It is emphasized that the value of the tuning parameter $\tilde{\phi}$ depends on the desired bandwidth via the experimental controller C^{exp} and the weighting filters.

For successful computation of the optimal order, the parametrization of the nominal model $\hat{P}(n_x)$ must be defined. In this chapter, the RMFD parametrization based on p.c.c. indices developed in Chapter 4 is used. Since a SISO system is considered, the p.c.c. index is equal to the considered model order n_x. Moreover, since the system is controlled through force actuation and position measurement, the minimal order at which the order selection procedure is executed is $n_{x,0} = 2$ and the order increment is 2.

7.3 Weighting filter design

In this subsection, the weighting filters are designed. As indicated in Chapter 6, loop-shaping-based weighting filters W_1 and W_2 are used. This type of filters allows shaping the open-loop response, i.e. $W_2 P_o W_1$, hence, it allows to specify a desired bandwidth. Furthermore, as the weighting filters can be incorporated into the closed-loop during controller synthesis, the weighting filters are allowed to contain integrators.

The open-loop should be shaped such that before the bandwidth f_{BW}, there is sufficient integral action. This is achieved by designing W_1 as follows,

$$W_1(s) = K \frac{s + 2\pi f_I}{s}, \qquad\qquad f_I = \frac{f_{BW}}{5}. \qquad (7.5)$$

To enforce controller roll-off, the weighting filter W_2 is designed as

$$W_2(s) = K \frac{1}{\frac{1}{2\pi f_R} s + 1}, \qquad\qquad f_R = 4 f_{BW}. \qquad (7.6)$$

The gain K is chosen such that the bandwidth of $W_2 P_o(j\omega) W_1$ is f_{BW}.

7.4 Controller

The experimental controller consists of integrator, lead-lag-filter and a low-pass filter. To avoid iterative identification and robust controller synthesis, the experimental controller is designed such that it is close to the optimal controller. Therefore, the experimental controller is designed with a bandwidth 15% under the desired bandwidth, i.e. $\tilde{f}_{BW} = 0.85 f_{BW}$. The controller blocks are then designed according to Table 7.1.

Table 7.1 Table indicating the pole-zero location of each controller block.

	Integrator	Lead-Lag	Lowpass
Pole	0	$2\tilde{f}_{BW}$	$10\tilde{f}_{BW}$
Zero	$\frac{\tilde{f}_{BW}}{10}$	$\frac{\tilde{f}_{BW}}{2}$	

7.5 Robust-Control-Relevant Model Set

The optimal model order highly depends on the specified bandwidth. Namely, a desired bandwidth sufficiently far away from the flexible dynamic behaviour means that accurate modelling of the flexible dynamic behaviour is less important for achieving robust performance. On the other hand, a desired bandwidth close to the flexible dynamic behaviour implies an increased model order, as in this case, accurate modelling of the flexible dynamic behaviour is important for achieving robust performance. Therefore, the framework developed in this research is applied in a simulation example for a large series of bandwidth-scenarios.

The robust-control-relevant model set identification with the order selection procedure is executed for a large variety of bandwidths, $f_{BW} = 10^{-2}$ Hz to $f_{BW} = 10^3$ Hz. The resulting optimal model orders are depicted in Figure 7.3. If the bandwidth is specified sufficiently far away from the resonant behaviour, the order selection criterion consistently selects a second-order nominal model. Therefore, only modelling the rigid-body behaviour results in a sufficiently tight model set $\mathcal{P}^{RCR}(n_x^*)$ in the frequency region which is relevant for control.

A larger model order is required if a bandwidth is selected near flexible dynamic behaviour, i.e. $0.6 < f_{BW} < 5$ Hz. In this case, only modelling the rigid-body behaviour is no longer sufficient, i.e. the first mode becomes performance limiting. As a result, the order selection criterion selects a fourth-order nominal model. This results in the robust-control-relevant model set $\mathcal{P}^{RCR}$ being sufficiently tight around the bandwidth.

If a bandwidth is specified within the flexible dynamic behaviour, $5 < f_{BW} < 250$ Hz, a fourth order nominal model is no longer sufficient, i.e. the second mode becomes performance limiting. For this reason, the order selection criterion consistently selects a sixth-order model. Therefore, a narrow model set $\mathcal{P}^{RCR}(n_x^*)$ in the control-relevant frequency region is only achieved by a high-order nominal model.

In the next subsections, the identification and order selection process will be elaborated for three bandwidth categories. That is, well before, just before the first mode and well after the last mode.
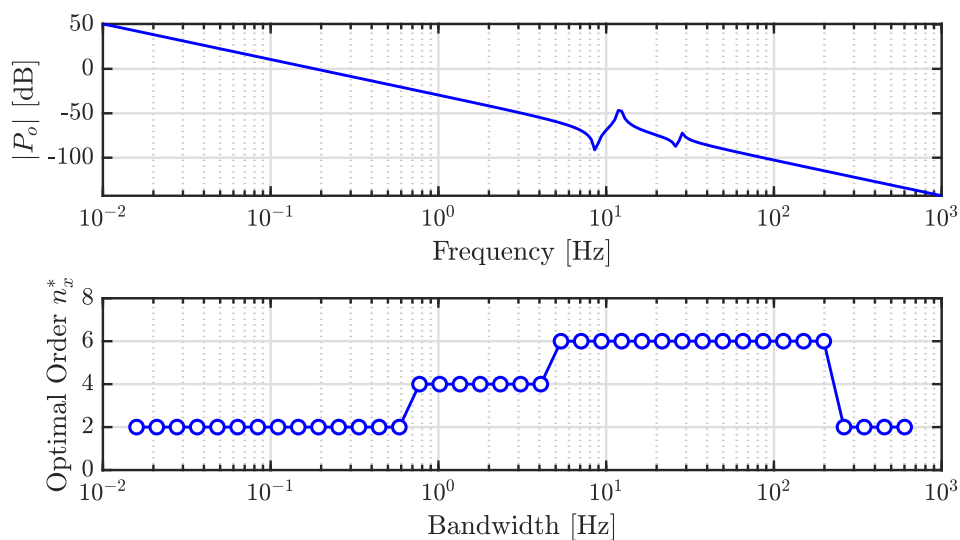
Figure 7.3 Optimal model order n_x^* as function of the desired bandwidth f_{BW}.

7.5.1 Pre Resonance

In this section, the identification of the model set $\mathcal{P}^{RCR}(n_x)$ and the order selection process is investigated for a desired bandwidth of $f_{BW} = 4.5 \cdot 10^{-1}$ Hz. To arrive at the robust-control-relevant model set, the coprime factors of the true system are computed using the FRF estimate of the true system P_o according to Eq. (5.2). The estimate is depicted in Figure 7.4.
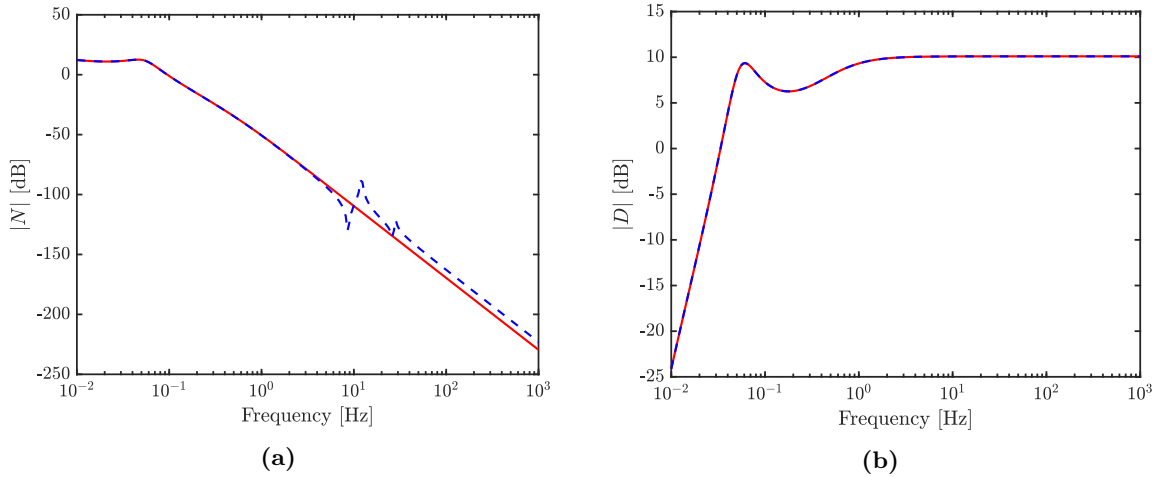
Figure 7.4 Bode magnitude diagram of the robust-control-relevant coprime factors: true system N_o, D_o (--) and the nominal model $\hat{N}, \hat{D}$ (−) for $n_x = 2$.

Using the coprime factors of the true system, the coprime factorization of the nominal model $\hat{P}(n_x)$ is computed by the algorithm proposed in Chapter 5. The resulting coprime factors are depicted in Figure 7.4. For conciseness, only a model order of $n_x = 2$ is shown. For frequencies in the vicinity of the target bandwidth, the coprime factors have a high gain. For frequencies far beyond the target bandwidth, the magnitude of the coprime factors is relatively low. Therefore, the dynamics which are relevant for control result in a high gain in the coprime factor domain.

A second step in the identification of the robust-control-relevant model set is the estimation of the size of the model uncertainty $\gamma(n_x)$. In this research, $\gamma(n_x)$ is determined by the approach discussed in Chapter 5. Based on the identified nominal model $\hat{P}(n_x)$ and the corresponding uncertainty magnitude $\gamma(n_x)$, the robust-control-relevant model is constructed,

$$\mathcal{P}^{RCR}(n_x) = \{P|P \text{ according to Definition 7}, \|\Delta_u\|_\infty \leq \gamma(n_x)\} . \tag{7.7}$$

To provide insight into the structure of the identified model set, the visualisation procedure proposed in [44] is adopted. The corresponding Bode diagrams of the model set $\mathcal{P}^{RCR}(n_x)$ for $n_x = 2, 4, 6$ are depicted in Figure 7.5. Around the target bandwidth, the model set is narrow and the nominal model accurately models the rigid-body independent of the selected model order. For a model order $n_x = 2$, the flexible dynamic behaviour is not modelled, hence, the uncertainty is large around the resonances. If a model order $n_x = 4$ is selected, the nominal model matches the true system quite well around the first mode. As a result, the model set is relatively small around the first mode. Due to the internal structure of the model set, i.e. the specific choice of coprime factors, the uncertainty is large at higher frequencies. If a model order $n_x = 6$ is selected, the nominal model matches the true system accurately, hence, the model set is narrow for all frequencies.
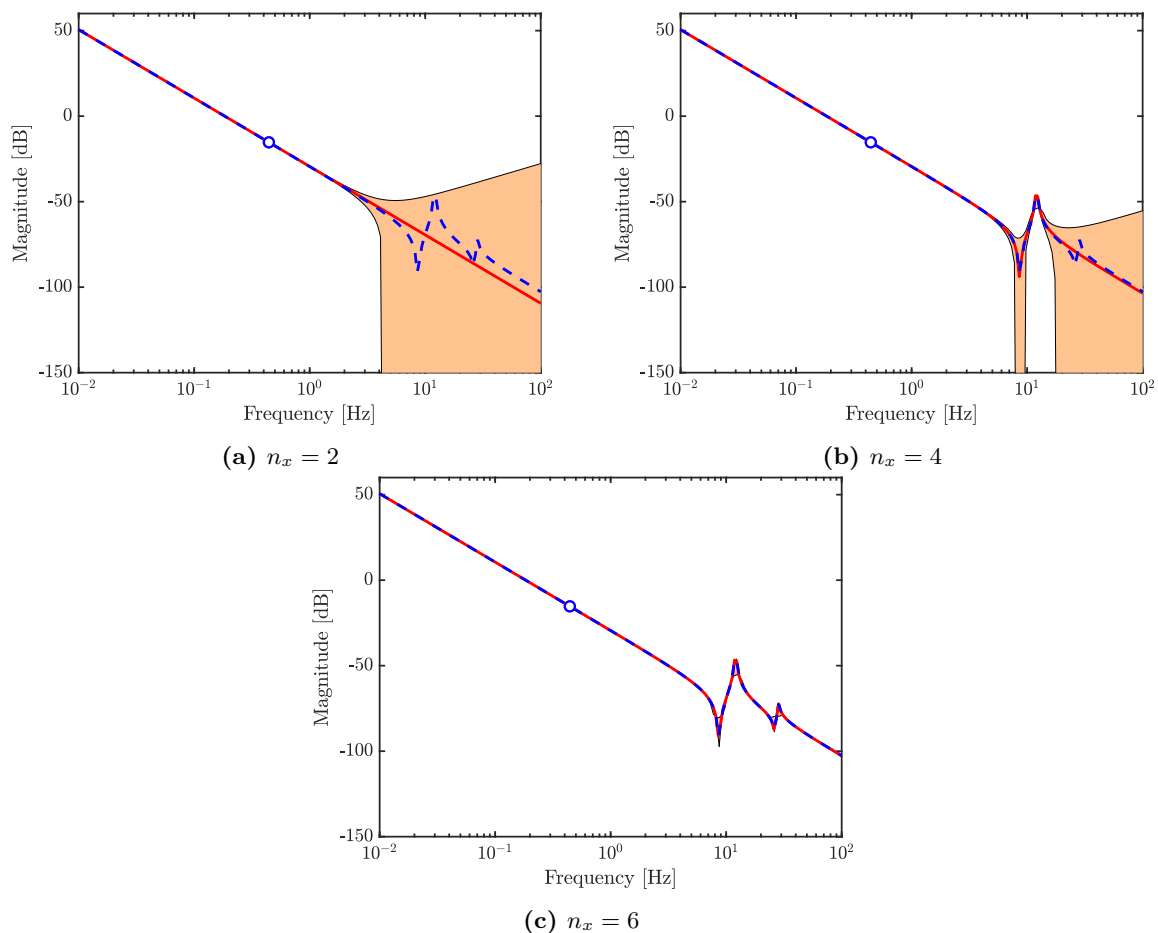
(a) $n_x = 2$

(b) $n_x = 4$

(c) $n_x = 6$

Figure 7.5 Bode magnitude diagram of the nominal model $\hat{P}(n_x)$ (–), the true system $P_o(n_x)$ (--) and the model set $\mathcal{P}^{RCR}(n_x)$(▨) for a model order $n_x = 2, 4, 6$. The desired bandwidth is indicated by (○).

Next, the worst-case performance is investigated with respect to the model set $\mathcal{P}^{RCR}(n_x)$. The performance of the robust-control-relevant model set $\mathcal{P}^{RCR}(n_x)$ in Table 7.2. Next, recall the important inequality for the construction of a robust-control-relevant model set,

$$\mathcal{J}(\mathcal{P}^{RCR}(n_x), C^{exp}) \leq \mathcal{J}(\hat{P}(n_x), C^{exp}) + \gamma(n_x). \tag{7.8}$$

It is verified that the inequality, Eq. (7.8), holds and is tight for all model orders. This shows that the model set is robust-control-relevant.

Table 7.2 Analysis of the robust-control-relevant model set for various model orders.

	$\gamma(n_x)$	$\mathcal{J}(P_o, C^{exp})$	$\mathcal{J}(\hat{P}(n_x), C^{exp})$	$\mathcal{J}(\mathcal{P}^{RCR}(n_x), C^{exp})$
$n_x = 2$	$4.0 \cdot 10^{-2}$	6.476	6.476	6.515
$n_x = 4$	$6.5 \cdot 10^{-4}$	6.476	6.476	6.476
$n_x = 6$	$7.0 \cdot 10^{-10}$	6.476	6.476	6.476

For the investigation of the optimal model order, the bound proposed in Theorem 2 is crucial,

$$\mathcal{J}_{WC}(\mathcal{P}^{RCR}(n_x), C^{exp}) \leq \mathcal{J}(P_o, C^{exp}) + 2\gamma(n_x). \tag{7.9}$$

When evaluating the worst-case performance, see Table 7.2, it is verified that Eq. (7.9) holds and is tight. This indicates that the order selection criterion is proposed in this research is nonconservative. Next, the optimal model order is investigated. The cost regarding the order selection criterion is calculated for $n_x = 2, 4, 6$. In Figure 7.6, the resulting cost evolution as function of the selected model order is depicted. Clearly, the minimum cost is achieved for a model order $n_x = 2$. Therefore, enlarging the model order does not result in a significant performance increase of the resulting robust controller. The key reason is that the desired bandwidth is far away from the flexible dynamic behaviour. As a result, the model set is sufficiently narrow in the frequency region which is relevant for control.
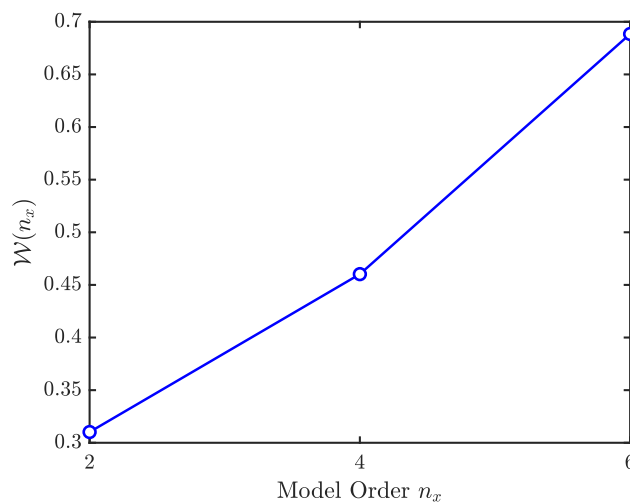
Figure 7.6 Cost function $\mathcal{W}(n_x)$.

7.5.2 Near Resonance

In this section, the optimal model order is investigated for a desired bandwidth of $f_{BW} = 3.5$ Hz. The investigation is concisely discussed, for an elaborate discussion on the order selection, the reader is referred to Section 7.5.1.

The cost regarding the order selection procedure $\mathcal{W}(n_x)$ is depicted for $n_x = 2, 4, 6$ in Figure 7.7. A minimal cost is achieved for $n_x = 4$. Therefore, if a bandwidth is selected near the resonant behaviour of the mechanical system, the first flexible mode becomes performance-limiting, hence a nominal model that only encompasses the rigid-body behaviour no longer suffices.

To provide insight into the structure of the robust-control-relevant model set with the optimal model order, the visualisation procedure proposed in [44] is adopted. The corresponding Bode diagram of the model set $\mathcal{P}^{RCR}(n_x^* = 4)$ is depicted in Figure 7.8. For frequencies near the target bandwidth, the nominal model $\hat{P}$ matches the true system P_o and the model set $\mathcal{P}^{RCR}$ is narrow. Secondly, the nominal model incorporates both the rigid-body behaviour and the first mode, therefore, the nominal model matches the true system accurately up to the second resonant mode. For frequencies beyond the first resonance, the model set is large. The same holds for frequencies below the target bandwidth. This particular shape is the result of the internal structure of the model set, i.e. the specific choice of coprime factors.
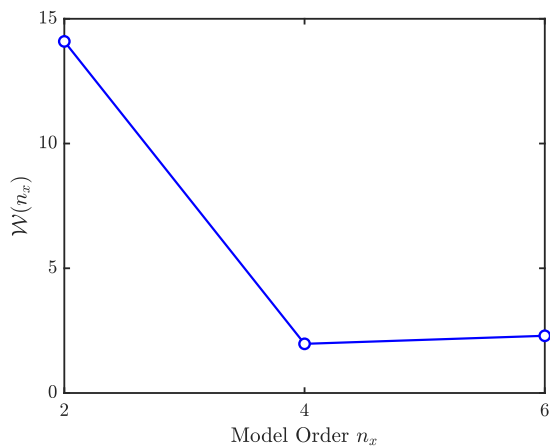
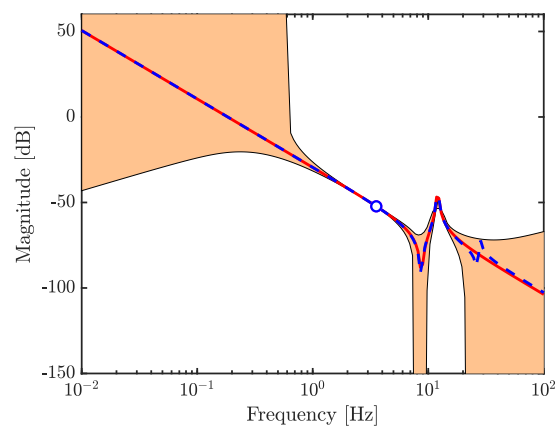**Figure 7.7** The cost regarding the model order selection $\mathcal{W}(n_x)$ for $n_x = 2, 4, 6$.

Figure 7.8 Bode magnitude diagram of the nominal model $\hat{P}(n_x^*)$ ($-$), the true system P_o ($--$) and the model set $\mathcal{P}^{RCR}(n_x^* = 4)$(■). The desired bandwidth is indicated by (○).

7.5.3 Post Resonance

In this section, the optimal model order is investigated for a desired bandwidth of $f_{BW} = 345$ Hz. The investigation will be concisely discussed, for an elaborate discussion on the order selection, the reader is referred to Section 7.5.1.

The cost regarding the order selection procedure $\mathcal{W}(n_x)$ is depicted for $n_x = 2, 4, 6$ in Figure 7.9. A model order of $n_x = 2$ achieves the minimal cost, hence the optimal model order $n_x^* = 2$. Therefore, incorporating the flexible dynamic in the nominal model does not result in a significant performance increase of the resulting robust controller. Hence, the selected bandwidth is sufficiently far away from the resonant behaviour, therefore, modelling only the rigid-body behaviour suffices for controller synthesize.

To provide insight into the structure of the robust-control-relevant model set with the optimal model order, the visualisation procedure proposed in [44] is adopted. The corresponding Bode diagram of the model set $\mathcal{P}^{RCR}(n_x^* = 2)$ is depicted in Figure 7.10. As a result of the control-relevant identification procedure, the nominal model accurately describes the post-resonant behaviour of the true system. As a result, in the vicinity and beyond of the bandwidth, the model set $\mathcal{P}^{RCR}$ is narrow. Before and during the flexible dynamic behaviour, the model set is large. This particular shape is the result of the internal structure of the model set.
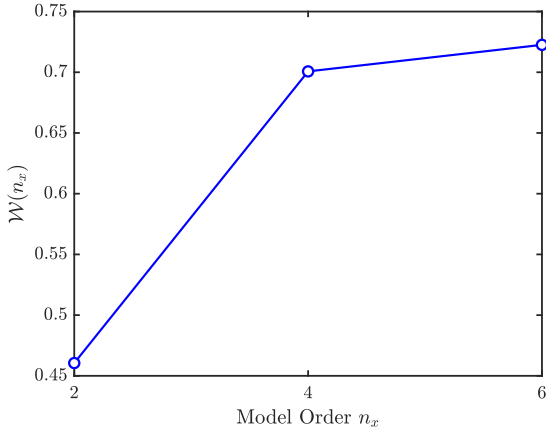
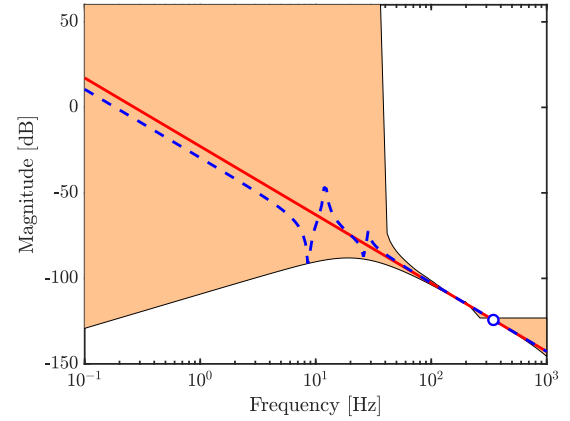**Figure 7.9** The cost regarding the model order selection $\mathcal{W}(n_x)$ for $n_x = 2, 4, 6$.

Figure 7.10 Bode magnitude diagram of the nominal model $\hat{P}(n_x^*)$ (–), the true system P_o (--) and the model set $\mathcal{P}^{RCR}(n_x^* = 2)$(■). The desired bandwidth is indicated by (○).

7.6 Robust Controller Synthesis

In this section, the robust controller is synthesized by using the robust-control-relevant model set with optimal model order $\mathcal{P}^{RCR}(n_x^*)$ discussed in the previous section. The synthesize of the robust controller is performed for the three bandwidth cases as discussed in Sections 7.5.1 to 7.5.3. The robust controller synthesis procedure is in accordance with Chapter 6.

7.6.1 Pre-Resonance

In this section, a robust controller is synthesized with a specified bandwidth of $f_{BW} = 4.5 \cdot 10^{-1}$ Hz using the model set with optimal model order $\mathcal{P}^{RCR}(n_x^* = 2)$ as discussed in Section 7.5.1.

The performance of the initial experimental controller C^{exp} and the robust controller C^{RP} is shown in Table 7.3. Clearly, the robust controller outperforms the experimental controller as the worst-case performance is significantly lower. Moreover, the robust controller enables a bandwidth equal to the specified bandwidth. It is emphasized that performance measures of Table 7.3 cannot be compared to the performance measures of the previous sections as different weighting filters are considered.

Table 7.3 Performance of the experimental and the robust controller.

	f_{BW} [Hz]	$\mathcal{J}(P_o, C)$	$\mathcal{J}(\hat{P}(n_x^*), C)$	$\mathcal{J}(\mathcal{P}^{RCR}(n_x^*), C)$
C^{exp}	$3.7 \cdot 10^{-1}$	6.476	6.476	6.515
C^{RP}	$4.4 \cdot 10^{-1}$	3.434	3.434	3.454

Figure 7.11, depicts the Bode diagram of the experimental controller C^{exp} and the robust controller C^{RP}. Clearly, the open-loop weighting filters successfully enforce controller roll-off and integral action. Interestingly, although a first-order low-pass filter is specified in the weighting filter design in Section 7.3, the robust controller contains a second-order low-pass filter. In Figure 7.12, the Bode diagram of the open-loop PC^{RP} and the shaped nominal plant $W_1\hat{P}W_2$ are depicted. The open-loop system indeed contains integral action and roll-off. However, around

the cross-over frequency, the open-loop system deviates significantly from the shaped system. This is explained by the phase of the shaped system being approximately $-200°$ around the cross-over frequency. As this leads to an unstable closed-loop system, the robust controller creates phase lead in the vicinity of the bandwidth which results in a decent phase margin.
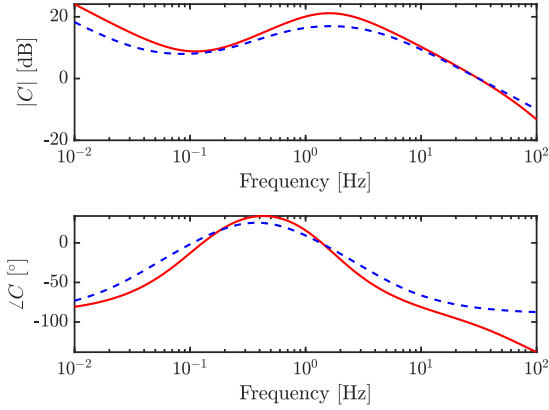

Figure 7.11 Bode diagram of the experimental controller C^{exp} (--) and the robust controller C^{RP} (–).
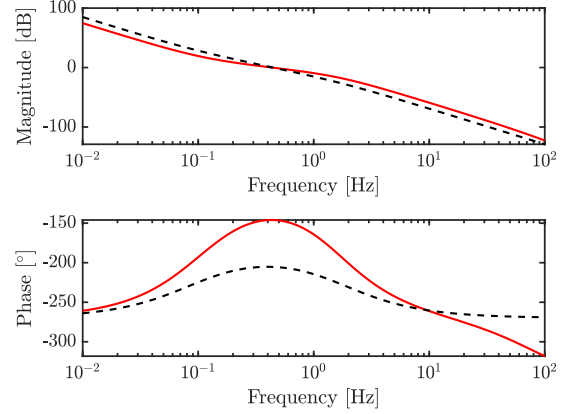
Figure 7.12 Bode diagram of the weighted nominal model $W_1 \hat{P} W_2$ (--) and the open-loop $\hat{P} C^{RP}$ (–).

Next, the performance of the robust controller C^{RP} is further evaluated by considering the Nyquist diagram for both the nominal and true system in Figure 7.17. The loop-gains do not encircle the point -1, hence according to Nyquist's theorem, the system is closed-loop stable [54]. Next, consider the sensitivity $(1 + P_o C)^{-1}$ and $(1 + \hat{P} C)^{-1}$ for C^{exp} and C^{RP} in Figure 7.14. Observe that the nominal and true sensitivity are approximately equal. Second, enforcing integral action and the increase in bandwidth from C^{exp} to C^{RP} result in enhanced disturbance suppression properties for low frequencies.
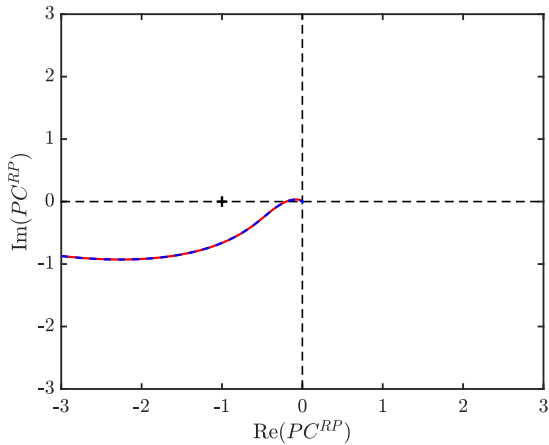

Figure 7.13 Nyquist diagram for the robust controller C^{RP} with the nominal model $\hat{P}(n_x^*)$ (–) and the true system P_o (--).
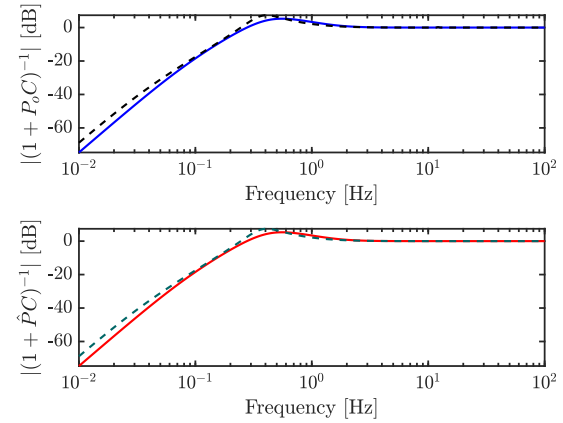

Figure 7.14 Bode magnitude diagram of the sensitivity $(1 + PC)^{-1}$. Top: sensitivity for the true system with C^{RP} (–) and C^{exp} (--). Bottom: sensitivity for the nominal system with C^{RP} (–) and C^{exp} (--).

7.6.2 Near-Resonance

In this section, a robust controller is synthesized with a specified bandwidth of $f_{BW} = 3.5$ Hz using the model set with optimal model order $\mathcal{P}^{RCR}(n_x^* = 4)$ as discussed in Section 7.5.2.

The performance of the initial experimental controller C^{exp} and the robust controller C^{RP} is depicted in Table 7.4. The worst-case performance with respect to the robust controller is significantly reduced. Moreover, the robust controller increases the bandwidth significantly compared to the experimental controller C^{exp}. However, to be robust against modelling errors, the controller does not achieve the specified bandwidth of $f_{BW} = 3.5$ Hz.

Table 7.4 Performance of the experimental and the robust controller.

	f_{BW} [Hz]	$\mathcal{J}(P_o, C)$	$\mathcal{J}(\hat{P}(n_x^*), C)$	$\mathcal{J}(\mathcal{P}^{RCR}(n_x^*), C)$
C^{exp}	3.0	8.511	8.513	8.733
C^{RP}	3.4	4.816	4.869	5.566

Figure 7.15 depicts the Bode diagram of the experimental controller C^{exp} and the robust controller C^{RP}. The open-loop weighting filters successfully enforce controller roll-off and integral action. The bode diagram of the open-loop PC^{RP} and the shaped nominal plant $W_1\hat{P}W_2$ is depicted in Figure 7.16. Observe that the shaped system leads to an unstable closed-loop system as at the cross-over frequency, the phase is approximately $-200°$. For this reason, the robust controller creates phase lead in the vicinity of the bandwidth which results in a decent phase margin. Second, around the first resonance, the robust controller mitigates the effect of the first resonance to ensure stability for the complete model set.
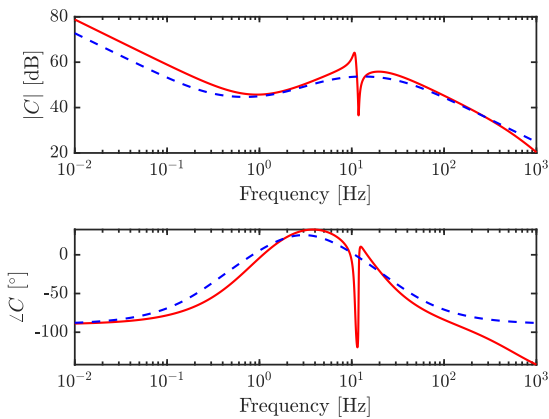

Figure 7.15 Bode diagram of the experimental controller C^{exp} (- -) and the robust controller C^{RP} (—).
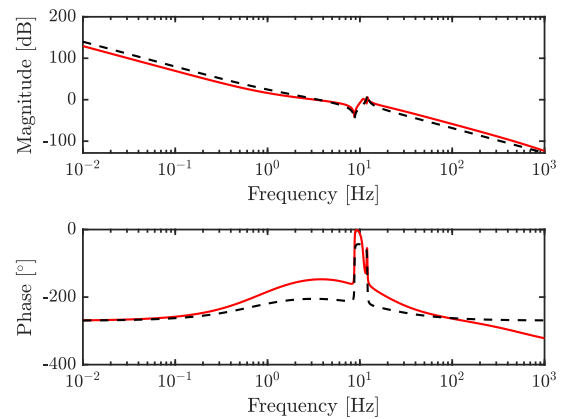
Figure 7.16 Bode diagram of the weighted nominal model $W_1\hat{P}W_2$ (- -) and the open-loop $\hat{P}C^{RP}$ (—).

Next, the performance of the robust controller C^{RP} is further evaluated by considering the Nyquist diagram for both the nominal and true system in Figure 7.17. In the vicinity of the resonance phenomena, the magnitude of the of P_oC^{RP} and $\hat{P}C^{RP}$ is larger than one. However, the phase of the loop-gains is such that the loop-gains do not encircle the point -1. Therefore, according to Nyquist's theorem, the system is closed-loop stable [54]. Next, consider the sensitivity $(1 + P_oC)^{-1}$ and $(1 + \hat{P}C)^{-1}$ for C^{exp} and C^{RP}. First of all, observe that the nominal

and true sensitivity are approximately equal. Second, enforcing integral action and the increase in bandwidth from C^{exp} to C^{RP} results in enhanced disturbance suppression properties for low frequencies.
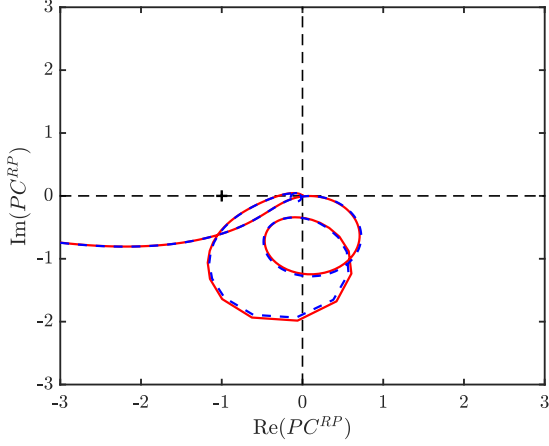

Figure 7.17 Nyquist diagram for the robust controller C^{RP} with the nominal model $\hat{P}(n_x^*)$ (–) and the true system P_o (--).
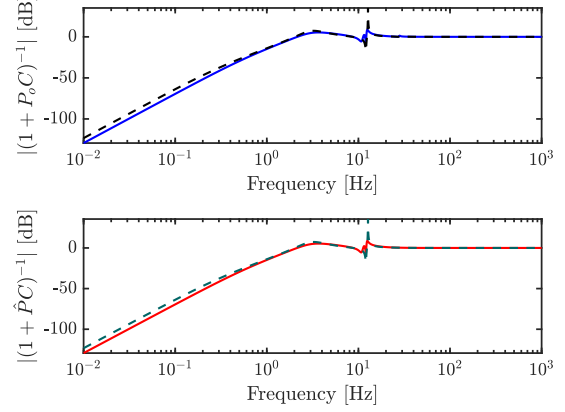
Figure 7.18 Bode magnitude diagram of the sensitivity $(1 + PC)^{-1}$. Top: sensitivity for the true system with C^{RP} (–) and C^{exp} (--). Bottom: sensitivity for the nominal system with C^{RP} (–) and C^{exp} (--).

7.6.3 Post-Resonance

In this section, a robust controller is synthesized with a specified bandwidth of $f_{BW} = 345$ Hz using the model set with optimal model order $\mathcal{P}^{RCR}(n_x^* = 2)$ as discussed in Section 7.5.3.

The performance of the initial experimental controller C^{exp} and the robust controller C^{RP} are depicted in Table 7.5. The worst-case performance concerning the robust controller is significantly lower than the performance with respect to the initial experimental controller. Moreover, the robust controller enables a bandwidth equal to the specified bandwidth. It is emphasized that the bandwidth is determined with respect to the true system P_o.

Table 7.5 Performance of the experimental and the robust controller.

	f_{BW} [Hz]	$\mathcal{J}(P_o, C)$	$\mathcal{J}(\hat{P}(n_x^*), C)$	$\mathcal{J}(\mathcal{P}^{RCR}(n_x^*), C)$
C^{exp}	293	6.662	6.662	6.771
C^{RP}	345	3.889	3.897	4.065

Figure 7.19 depicts the Bode diagram of the experimental controller C^{exp} and the robust controller C^{RP}. The open-loop weighting filters successfully enforce controller roll-off and integral action. The bode diagram of the open-loop PC^{RP} and the shaped nominal plant $W_1\hat{P}W_2$ is depicted in Figure 7.20. At the cross-over frequency, the phase of $W_1\hat{P}W_2$ is approximately $-200°$. Therefore, to enables a stable closed-loop, the robust controller creates phase lead in the vicinity of the bandwidth which results in a decent phase margin.
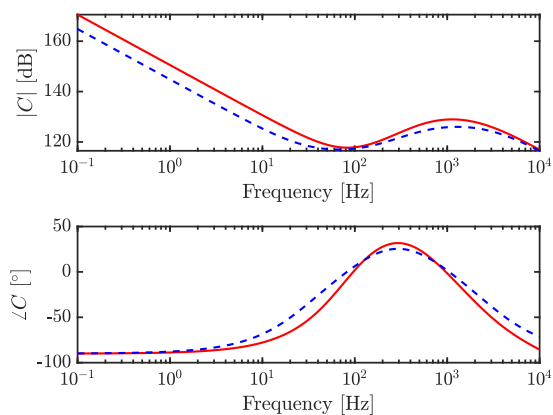
Figure 7.19 Bode diagram of the experimental controller C^{exp} (- -) and the robust controller C^{RP} (–).
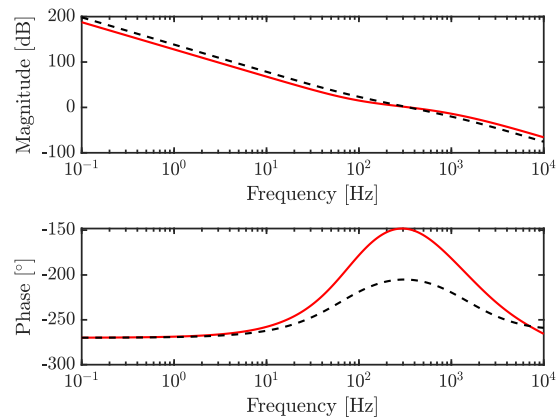

Figure 7.20 Bode diagram of the weighted nominal model $W_1 \hat{P} W_2$ (- -) and the open-loop $\hat{P} C^{RP}$ (–).

The performance of the robust controller C^{RP} is further evaluated by considering the Nyquist diagram for both the nominal and true system in Figure 7.17. As the bandwidth is far beyond the resonance phenomena and there is sufficient phase margin, the loop-gains do not encircle the point -1. Therefore, according to Nyquist's theorem, the system is closed-loop stable [54]. Next, consider the sensitivity $(1 + P_o C)^{-1}$ and $(1 + \hat{P} C)^{-1}$ for C^{exp} and C^{RP}. As the nominal model does not incorporate the resonance phenomena, the sensitivity with respect to the nominal model deviates from the true sensitivity for frequencies near the resonance phenomena. For frequencies beyond and below the resonance phenomena, the sensitivity with respect to the nominal model mimics the true sensitivity quite well. Next, observe that enforcing integral action and the increase in bandwidth from C^{exp} to C^{RP} result in enhanced disturbance suppression properties for low frequencies.
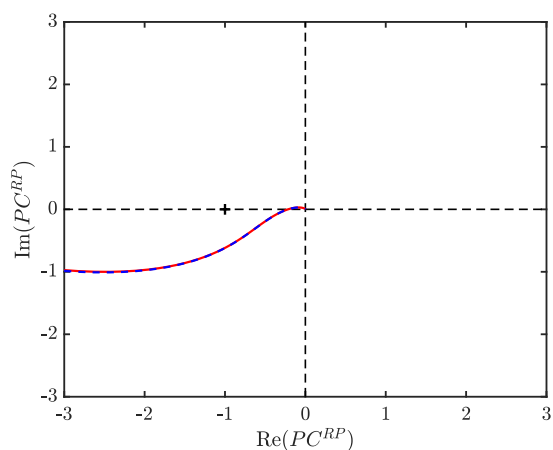

Figure 7.21 Nyquist diagram for the robust controller C^{RP} with the nominal model $\hat{P}(n_x^*)$ (–) and the true system P_o (- -).
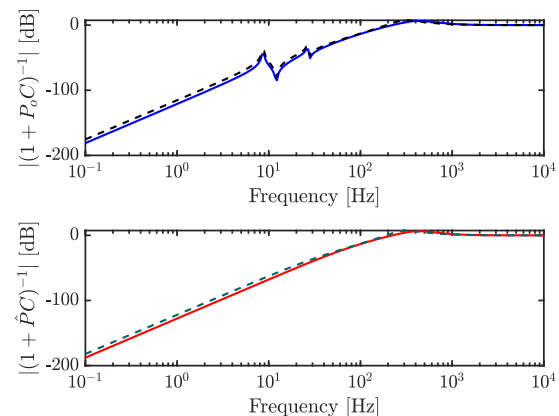

Figure 7.22 Bode magnitude diagram of the sensitivity $(1 + PC)^{-1}$. Top: sensitivity for the true system with C^{RP} (–) and C^{exp} (- -). Bottom: sensitivity for the nominal system with C^{RP} (–) and C^{exp} (- -).

7.7 Overview

In this chapter, a SISO mechanical system is considered to which the joint identification and robust controller synthesis framework with model order selection is successfully applied.

First, the identification of the robust-control-relevant model set is executed with the model order selection proposed in this research for various bandwidth scenarios. It is shown that if a bandwidth is selected well ahead or well after the flexible dynamic behaviour, a nominal model describing only the rigid-body behaviour is sufficient for achieving high performance. If bandwidth is selected just before the flexible dynamic behaviour, the first flexible mode becomes performance limiting. Therefore, using a robust-control-relevant model set with a low order is sufficient for achieving a high performance. The usage of model order selection procedure for robust-control-relevant model sets extends to existing methods for the identification for robust control purposes where typically high model orders are considered which hampers successful implementation in a real-time environment [60, 47].

In the second part, using the robust-control-relevant model set with optimal model order, the robust controllers are successfully synthesized. It is shown that robust controllers in conjunction with the robust-control-relevant model set achieve high performance. For future work, it is recommended to consider a MIMO system, as an even larger performance increase is expected as robust control is able to deal with inherently multivariable systems.

Chapter 8

Conclusion & Recommendation

8.1 Conclusion

In this research, a framework is developed for control of next-generation motion stages. The developed framework is specifically suitable for next-generation motion systems which are envisioned to contain many inputs and outputs. In addition, it is expected that the flexible dynamic behaviour is present within the control bandwidth resulting in an inherently multivariable system. The developed framework contains all steps from model set identification to robust controller synthesis.

For the synthesis of a robust controller that leads to a high performance, the identification of a nonconservative model set is crucial. To enable the construction of a nonconservative model set, the dual-Youla-Kučera model structure is adopted. More specifically, the freedom in the coprime factorizations that constitute the dual-Youla-Kučera uncertainty structure are exploited in Chapter 3. This specific factorization enables tractable identification of a robust-control-relevant model set. In addition, the factorization allows the usage of unstructured perturbations which leads to a nonconservative synthesis of the robust controller in Chapter 6. This is in contrast to existing methods, which use structured uncertainty blocks, and result in conservatism in the synthesis of the robust controller.

To facilitate robust feedback control with low computational complexity, the order of the controller should be small. Consequently, a low-order model should be identified. This is accomplished by the introduction of a regularization term which penalizes the model order of the nominal model in Chapters 2 and 3. By exploiting the freedom of the coprime factors, a novel connection between the performance and the selected model order is derived in Chapter 3. This connection in combination with the regularization term enables to efficiently manage the tradeoff between model order and the performance of the resulting robust controller.

To enable a model order selection procedure, an RMFD parametrization is adopted that enables the parametrization of a rich class of mechanical systems through the usage of pseudo-canonical indices in Chapter 4. To enable successful numerical estimation of the model set, a numerical routine is developed in Chapter 5.

The framework for next-generation motion control is successfully applied to a simulation example

in Chapter 7. The simulation proved the usefulness of the model order selection procedure, as for a bandwidth far or close to the flexible dynamic behaviour, a low-order nominal model suffices for synthesising a robust controller that leads to a high performance. The usage of the model order selection procedure extends to existing methods regarding system identification for robust control where typically high model orders are selected which hampers successful implementation in a real-time environment [60, 47].

8.2 Recommendation

For future research, some additional topics can be addressed.

- The joint identification and robust controller synthesis framework with model order selection is tailored towards systems with many inputs and outputs. Therefore, in future research, it is recommended to extend the simulation discussed in Chapter 7 to a MIMO system. As robust controllers can effectively deal with inherently multivariable systems, it is expected that the robust control strategy outperforms conventional loop-shaping-based controllers. The simulations can be used to experimentally prove this hypothesis. It is emphasized that the proposed framework is particularly suitable for MIMO systems and that only the simulations need to be extended towards a MIMO case.

- Also, if the joint identification and robust controller synthesis framework is applied to a MIMO simulation, the RMFD parametrization with respect to the generic controllability index and the specific controllability index can be compared to see which index is preferable in an experimental setting.

- Regarding the experimental FFR-setup, it is recommended to perform FRF measurements and to apply the framework for next-generation motion control to the FFR setup. This could give experimental evidence of the performance increase of the robust controller with respect to a conventional loop-shaping-based controller.

- In addition, the rigid-body decoupled FFR setup does not show the typical collocated behaviour, i.e. the Bode diagram indicates that the first resonance occurs before the first anti-resonance. Therefore, the simulations performed in Chapter 7, can be repeated for a system where resonance occurs before the anti-resonance. By comparing the optimal model order as function of the bandwidth, new insights can be generated on the relevance of modelling flexible dynamic behaviour.

Appendix A

Reticle Stage Setup

A.1 General

In Figure A.1, the FFR is schematically shown with its main components. The setup consists of two independently controlled systems. The first system is the active vibration isolation system. It consists of a base frame which is mounted to the floor. On top of the base frame, a metrology frame is mounted which is weakly suspended by air mounds. To enhance vibration isolation properties, also Lorentz actuators are mounted to actively suppress disturbances. For more details on this part of the setup, see [9]. The second system is the reticle stage. The position of the reticle stage is measured with respect to the metrology frame. The actuation is performed relative to the base frame.
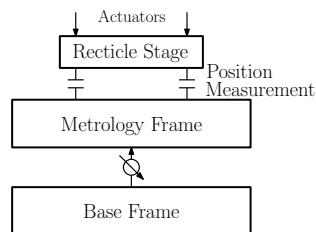

Figure A.1 Figure indicating a schematic overview of the FFR setup.
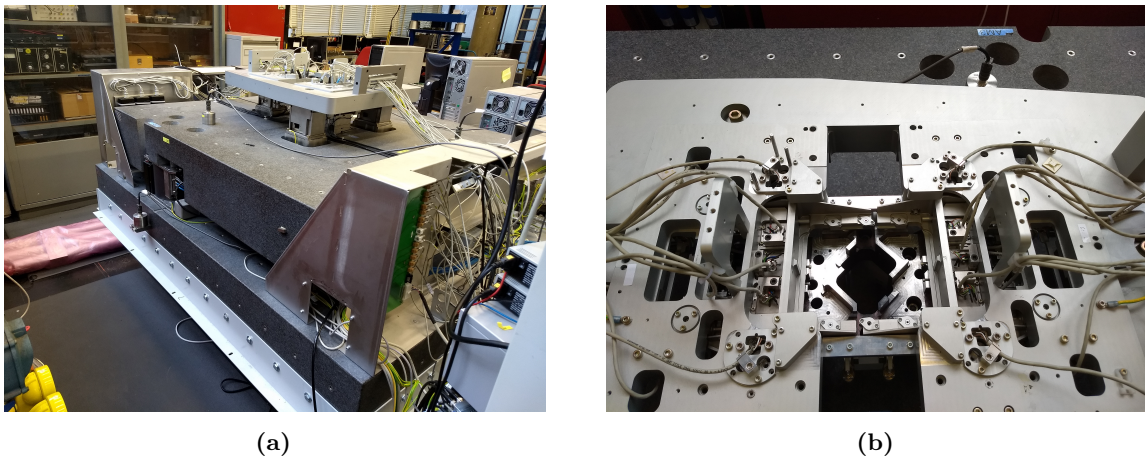
(a) **(b)**

Figure A.2 (a) Over view of the FFR setup. (b) Figure showing the reticle stage.

The goal of the FFR setup is to accurately position the reticle stage in 6 DOFs. The reticle stage consists of two so-called actuator bodies which can be controlled independently of each other. Originally, the actuator bodies were coupled through a reticle, however, for practical reasons, these are now coupled by two stiff aluminum beams. The current solid actuator body can be positioned in 6 DOFs using 14 actuators and 14 sensors. four sensors and actuators in the x-directions, two sensors and actuators in the y direction and 8 in the z-direction of which four actuators are equipped with a permanent magnet to compensate for the gravitational force of the reticle stage. In Figure A.3 the position of each actuator and sensor in the reticle stage is shown.
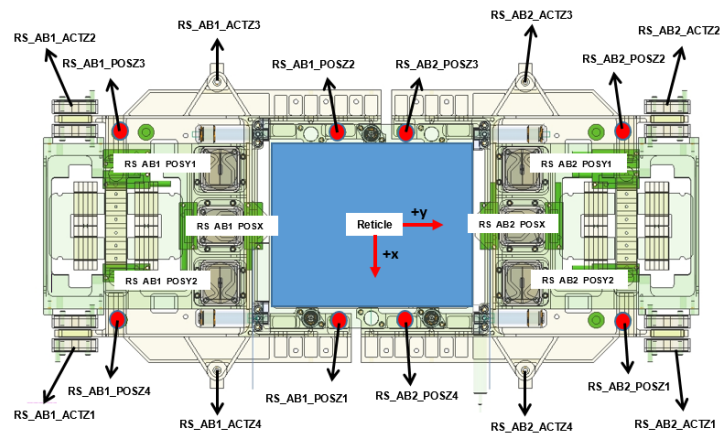

Figure A.3 Figure indicating a schematic overview of the FFR setup [36].

The actuators used to position the reticle are so-called Lorentz actuators. It consists of two coils above and below a permanent magnet. The coils are fixed to the base frame and the permanent magnet is attached to the reticle stage. The control input for the actuators should be between $U = \{U \in \mathbb{R} | -10 \leq U \leq 10\}$ V.

The position in the z-direction is measured with capacitive sensors of PI. The position in x- and y-direction is measured by Renishaw encoders.

An FRF measurement of the rigid-body-decoupled for the z, R_x, R_y -direction is given in Figure A.4. Interestingly, the frequency response function indicates that the resonance occurs before the anti-resonance. Therefore, it deviates from the classical collocated behaviour. The collocated behaviour might be lost because of the rigid-body decoupling which reduces 14 inputs and outputs to 6 inputs and 6 outputs.
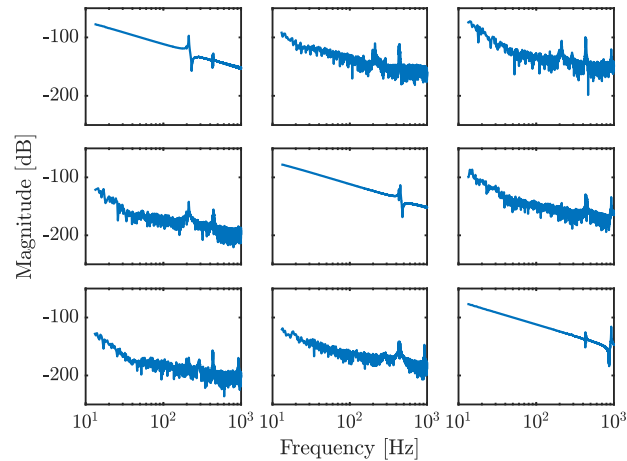

Figure A.4 Bode magnitude diagram of FRF of the z, R_x and R_y of the FFR setup [59].

A.2 Calibration

To measure the position from a relevant coordinate frame, the position-sensors must be calibrated. First, the calibration of z-direction is discussed, thereafter, the x- and y-direction calibration is discussed.

A.2.1 z-position

The position in the z-direction is measured using capacitive sensors of PI. These sensors are absolute, i.e. they do not require an offset to be compensated in the software. However, these sensors require mechanical calibration. Each sensor is equipped with a manipulator with which the height of each sensor can be adjusted. This is shown in figure Figure A.5. The height should be adjusted such that all z-sensors are in the same plane. However, these manipulators are not accurate enough, therefore, they are approximately within the same plane. Then, a homing procedure is executed. The actuators pull the reticle stage downwards then based on this position values of the sensor the offset of each z-sensors is computed. This homing procedure is executed before each experiment.
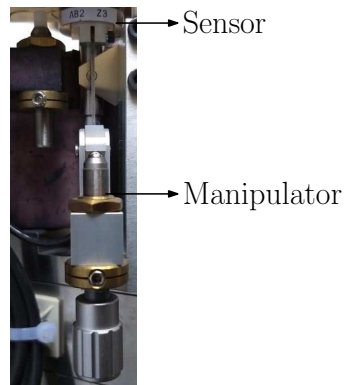
Figure A.5 Figure indicating the capacitive sensors with a manipulator.

A.2.2 xy-position

The position in x- and y-direction is measured using Renishaw encoders. These sensors essentially count the number of increments with which the position is determined. Therefore, they require a homing procedure. This homing procedure essentially follows the following steps. (1) The z-direction is controlled and the reticle stage is floating. (2) The x- and y -actuators push the reticle stage in the corner. (3) Determine the offset. The homing procedure is executed before each experiment.

The quality the sensor output is determined by the so-called sin-cos signals, see [35, 33] for a detailed explanation. The quality of the signal is determined by distance and angle between the encoder readhead and the increments. For this reason, correct z-calibration is essential. The quality of the encoder signal can be seen on the encoder plug. Currently, a quality of 3 out 5 can be reached. Although this is certainly not optimal, the reticle stage can be controlled using this sensor signal quality.

A.2.3 Reparations

In previous research, two sensors and three actuators were broken. In this research, the broken sensors are replaced and the actuators are repaired. The malfunctioning of the actuators has to do with a design issue. This resulted in broken wires and short circuits. To prevent this from happening again, each actuator is equipped with a so-called strain relief. This is shown in Figure A.6.
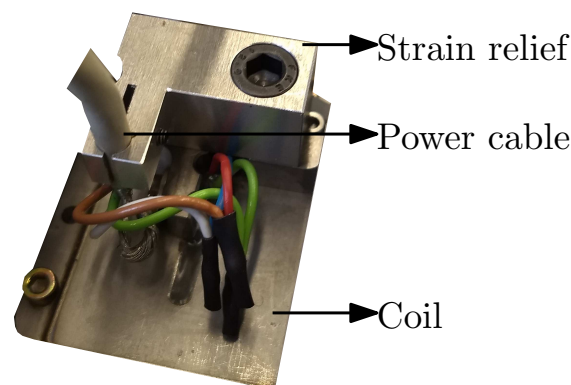

Figure A.6 Figure indicating the actuator-coil and strain relief.

A.2.4 Actuators

The actuators are steered through two wires. However, during the assembling of the setup, some of these wires are connected in the opposite manner which means that the actuation is performed in the wrong direction. Therefore, the direction of each actuator is checked and compensated through a minus-sign in the software if necessary.

A.2.5 Experimental Controller

For experiments, an experimental controller must be designed. As the plant contains 14 sensor-actuator pairs, finding an initial controller for this is difficult. Therefore, a rigid-body decoupling is performed, to reduce the amount of control input-output pairs to 6. In this research, the rigid-body decoupling and initial controller found in is used, see [59].

A.3 Simulink Implementation

In Figure A.7, the Simulink model is presented. From this figure, it can be seen that the model consists of two parts. The first part is the control of the active vibration isolation part, see [9]. This part is implemented in a consistent and sustainable manner, therefore, this part is reused in this work. The second part is the control of the reticle stage see [36, 59, 65]. This part is implemented in an inconsistent manner. Therefore, in this research, this part is programmed again, resulting in a sustainable and modular Simulink model.
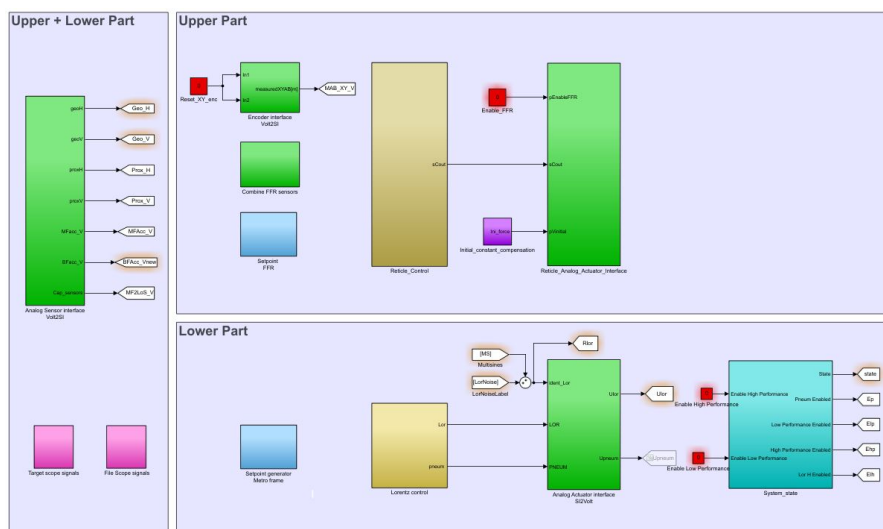

Figure A.7 Simulink implementation of the FFR control architecture.

Appendix B

Proofs

B.1 Proof: Theorem 2

Proof. Recall the worst case performance bound of Eq. (3.21),

$$\mathcal{J}_{WC}(\mathcal{P}^{RCR}, C^{exp}) \leq J(\hat{P}, C^{exp}) + \gamma. \tag{B.1}$$

Next, consider the triangular inequality [51, 3],

$$\mathcal{J}(\hat{P}, C^{exp}) \leq J(P_o, C^{exp}) + \gamma \tag{B.2}$$

Combining Eq. (B.1) and (B.2) proves Theorem 2. $\qquad \square$

B.2 Proof: Theorem 3

Proof. To proof Theorem 3, recall that the state space representation of a generally damped system equals,

$$\left[\begin{array}{c|c} A & B \\ \hline C & 0 \end{array} \right] = \left[\begin{array}{cc|c} O & I & o \\ -\Omega^2 & -D_m & \mathcal{R} \\ \hline \mathcal{L} & o & \end{array} \right] \tag{B.3}$$

Next, consider the zeroth order derivative of the output,

$$y = Cx \tag{B.4}$$

It can be seen that the expression above does not depend on the output u. Therefore, consider the first order derivative,

$$\dot{y} = C\dot{x} \tag{B.5}$$

$$\dot{y} = CAx + CBu \tag{B.6}$$

$$\dot{y} = CAx \tag{B.7}$$

Herein, $CB = 0$ because of the specific structure of a mechanical system, Eq. (B.3). Next, consider the second order derivative,

$$\ddot{y} = C\ddot{x} \tag{B.8}$$

$$\ddot{y} = CA^2x + CABu \tag{B.9}$$

$$\tag{B.10}$$

Where CAB is defined as,

$$CAB = \mathcal{L}\mathcal{R} \tag{B.11}$$

$\square$

This matrix is nonzero if each DOF is actuated and measured, e.g. collocated control. This proves Theorem 3.

B.3   Proof: Theorem 4

Proof. Note that generic controllability indices have the following structure $\delta = [\phi, ..., \phi, \phi - 1, ..., \phi - 1]$. Then the corresponding numerator indices are $\nu_i \in \{\phi - 1, ..., \phi - 1, \phi - 2, ..., \phi - 2\}$. As it holds that $\mu_i \geq \nu_i \forall i \in \{1, ..., n_u\}$, the transformation from pseudo canonical state space to RMFD is valid. Next, consider the degree structure for N and D,

$$\deg(D(s,\theta)) = \left[\begin{array}{ccc|ccc} \phi & & \phi - 1 & & & \\ & \ddots & & & \phi - 1 & \\ \phi - 1 & & \phi & & & \\ \hline & & & \phi - 1 & & \phi - 2 \\ & \phi - 2 & & & \ddots & \\ & & & \phi - 2 & & \phi - 1 \end{array} \right] \tag{B.12}$$

$$\deg(N(s,\theta)) = \left[\begin{array}{c|c} \phi - 2 & \phi - 3 \end{array} \right] \tag{B.13}$$

As Eq. (B.12) and (B.13) are column reduced, the relative degree can be obtained by comparing the column degrees. It can easily be seen that the relative degree is larger than two for all columns [65]. For the specific indices, the proof is similar and left to the reader. $\square$

B.4   Proof: Theorem 6

The proof is split into two parts, first consider the proof for the input transformation

Proof. Given the mechanical system Σ, $\frac{n_x}{n_y} \in \mathbb{N}$ and let $\mathcal{C} \in \mathbb{R}^{n_u n_x \times n_x}$ be the controllability matrix with δ_g the corresponding generic controllability indices. The controllability matrix can be partitioned according to $\mathcal{C} = \begin{bmatrix} \mathcal{C}_g & \mathcal{C}_h \end{bmatrix}$ with $\mathcal{C}_g = \{\mathcal{C}_g \in \mathbb{R}^{n_x \times n_x} | \text{rank}(\mathcal{C}_g) = n \leq n_x\}$. Next, consider the input transformation: $y = D\bar{y}$, with $\det(D) \neq 0$. Since $\frac{n_x}{n_y} \in \mathbb{N}$, the transformation matrix D is a block diagonal matrix with equal diagonal blocks. For this reason, the following holds

$$\text{rank}(\bar{\mathcal{C}}_g) = \text{rank}(\mathcal{C}_g D) = \text{rank}(\mathcal{C}_g) = n. \tag{B.14}$$

Hence, if for Σ holds that $\text{rank}(\mathcal{O}_g) < n_x$, this also holds for the output transformed system. $\square$

Now, consider the second part, the proof for the state transformation.

Proof. Given the mechanical system Σ, $\frac{n_x}{n_y} \in \mathbb{N}$ and let $\mathcal{C} \in \mathbb{R}^{n_u n_x \times n_x}$ be the controllability matrix with δ_g the corresponding generic controllability indices. The controllability matrix can

be partitioned according to $\mathcal{C} = \begin{bmatrix} \mathcal{C}_g & \mathcal{C}_h \end{bmatrix}$ with $\mathcal{C}_g = \{\mathcal{C}_g \in \mathbb{R}^{n_x \times n_x} | \text{rank}(\mathcal{C}_g) = n \leq n_x\}$. Next, consider the state transformation: $x = T\bar{x}$, with $\det(T) \neq 0$.

$$\text{rank}(\bar{\mathcal{C}}_g) = \text{rank}(T^{-1}\mathcal{C}_g) = \text{rank}(\mathcal{C}_g) = n. \tag{B.15}$$

Hence, if for Σ holds that $\text{rank}(\mathcal{O}_g) < n_x$, this also holds for the state transformed system. $\square$

B.5   Proof: Theorem 8

Proof. For the frobenius-norm, the following holds,

$$\|\Phi\|_F = \|\text{vec}(\Phi)\|_2. \tag{B.16}$$

Applying this equality to Eq. (5.6), leads to,

$$\sum_{k=1}^{N_\omega} \left\| \text{vec}\left(W_h^{<j>}(\xi_k) \circ \left(W\left(\begin{bmatrix} N_o(\xi_k) \\ D_o(\xi_k) \end{bmatrix} - \begin{bmatrix} \hat{N}(\xi_k, \theta) \\ \hat{D}(\xi_k, \theta) \end{bmatrix} \right) \right) \right) \right\|_2. \tag{B.17}$$

Applying the vectorization equality, $\text{vec}(A \circ B) = \text{diag}(\text{vec}(A))\text{vec}(B)$,

$$\sum_{k=1}^{N_\omega} \left\| \tilde{W}_h^{<j>} \text{vec}\left(W\left(\begin{bmatrix} N_o(\xi_k) \\ D_o(\xi_k) \end{bmatrix} - \begin{bmatrix} \hat{N}(\xi_k, \theta) \\ \hat{D}(\xi_k, \theta) \end{bmatrix} \right) \right) \right\|_2, \tag{B.18}$$

where, $\tilde{W}_h^{<j>} = \text{diag}(\text{vec}(W_h^{<j>}))$. Next, substituting Eq. (5.1) into the equation gives the following result,

$$\sum_{k=1}^{N_\omega} \left\| \tilde{W}_h^{<j>} \text{vec}\left(W\left(\begin{bmatrix} N_o(\xi_k) \\ D_o(\xi_k) \end{bmatrix} - \begin{bmatrix} B(\theta) \\ A(\theta) \end{bmatrix} \left(\tilde{D}_e A(\theta) + \tilde{N}_{e,2} V_2^{-1} B(\theta) \right)^{-1} \right) \right) \right\|_2 \tag{B.19}$$

Rearranging gives,

$$\sum_{k=1}^{N_\omega} \left\| \tilde{W}_h^{<j>} \text{vec}\left(W\left(\begin{bmatrix} N_o \tilde{N}_{e,2} V_2^{-1} & N_o \tilde{D}_e \\ D_0 \tilde{N}_{e,2} V_2^{-1} & D_o \tilde{D}_e \end{bmatrix} - I \right) \begin{bmatrix} B(\theta) \\ A(\theta) \end{bmatrix} \left(\tilde{D}_e A(\theta) + \tilde{N}_{e,2} V_2^{-1} B(\theta) \right)^{-1} \right) \right\|_2 \tag{B.20}$$

Next, using the vectorization equality, $\text{vec}(ABC) = (C^\top \otimes A)\text{vec}(B)$ the following can be derived,

$$\sum_{k=1}^{N_\omega} \left\| \tilde{W}_h^{<j>} \left(\left[\left(\tilde{D}_e A(\theta) + N_{e,2} V_2^{-1} B(\theta) \right)^{-1} \right]^\top \otimes \left[W\left(\begin{bmatrix} N_o \tilde{N}_{e,2} V_2^{-1} & N_o \tilde{D}_e \\ D_0 \tilde{N}_{e,2} V_2^{-1} & D_o \tilde{D}_e \end{bmatrix} - I \right) \right] \right) \text{vec} \begin{bmatrix} B(\theta) \\ A(\theta) \end{bmatrix} \right\|_2. \tag{B.21}$$

Thereby proving Theorem 8. $\square$

B.6   Proof: Theorem 9

Proof. The elements of $\hat{D}$ can be written as

$$[A(\xi_k, \theta)]_i^j = \delta(i, j)\xi_k^{\mu_i} - \begin{bmatrix} 1 & \xi_k & \cdots & \xi_k^{\mu_i - 1} \end{bmatrix} \begin{bmatrix} \alpha_{ji1} \\ \alpha_{ji2} \\ \vdots \\ \alpha_{ji\mu_i} \end{bmatrix}, \tag{B.22}$$

$$[B(\xi_k, \theta)]_i^j = - \begin{bmatrix} 1 & \xi_k & \cdots & \xi_k^{\nu_j - 1} \end{bmatrix} \begin{bmatrix} \beta_{ji1} \\ \beta_{ji2} \\ \vdots \\ \beta_{ji\nu_j} \end{bmatrix} \tag{B.23}$$

The elements of the polynomial matrices can also be grouped with respect to the columns

$$\begin{bmatrix} \left[B(\xi_k, \theta)\right]^j \\ \left[A(\xi_k, \theta)\right]^j \end{bmatrix} = \underbrace{\begin{bmatrix} 0 \\ \vdots \\ 0 \\ \hline \delta_{i1}\xi_k^{\mu_1} \\ \vdots \\ \delta_{in_u}\xi_k^{\mu_{n_u}} \end{bmatrix}}_{[b]_i} - \underbrace{\begin{bmatrix} & O & & F(\nu_j) & & O \\ & & & & \ddots & \\ & & & O & & F(\nu_j) \\ \hline F(\mu_1) & & O & & & \\ & \ddots & & & O & \\ O & & F(\mu_{n_u}) & & & \end{bmatrix}}_{\Phi_j} \underbrace{\begin{bmatrix} \alpha_j \\ \beta_j \end{bmatrix}}_{\theta_j} \tag{B.24}$$

As the vectorization operator essentially stacks the columns of $\begin{bmatrix} B(\xi_k, \theta) \\ A(\xi_k, \theta) \end{bmatrix}$, the proof of Theorem 9 is finished. $\qquad\square$

Appendix C

Code of Scientific Conduct

TU/e Technische Universiteit
Eindhoven
University of Technology

**Declaration concerning the TU/e Code of Scientific Conduct
for the Master's thesis**

I have read the TU/e Code of Scientific Conduct[1].

I hereby declare that my Master's thesis has been carried out in accordance with the rules of the TU/e Code of Scientific Conduct

Date

17 December 2019

Name

PJMM Toss

ID-number

0897675

Signature

Submit the signed declaration to the student administration of your department.

[1] See: http://www.tue.nl/en/university/about-the-university/integrity/scientific-integrity/
The Netherlands Code of Conduct for Academic Practice of the VSNU can be found here also.
More information about scientific integrity is published on the websites of TU/e and VSNU

January 15 2016

Bibliography

[1] A. A. Agrachev and Y. Sachkov. *Control theory from the geometric viewpoint*, volume 87. Springer Science & Business Media, 2013.

[2] H. Akaike. Information theory and an extension of the maximum likelihood principle. In *Selected papers of hirotugu akaike*, pages 199–213. Springer, 1998.

[3] P. Albertos and A. S. Piqueras. *Iterative identification and control: advances in theory and applications*. Springer Science & Business Media, 2012.

[4] B. D. Anderson. From youla–kucera to identification, adaptive and nonlinear control. *Automatica*, 34(12):1485–1506, 1998.

[5] D. S. Bayard. Multivariable frequency domain identification via 2-norm minimization. In *Proceedings American Control Conference*, pages 1253–1257. IEEE, 1992.

[6] D. S. Bayard. High-order multivariable transfer function curve fitting: Algorithms, sparse matrix methods and experimental results. *Automatica*, 30(9):1439–1444, 1994.

[7] D. S. Bayard and R. Y. Chiang. Identification, uncertainty characterization and robust control synthesis applied to large flexible structures control. *International Journal of Robust and Nonlinear Control*, 8(2):97–112, 1998.

[8] M. Beijen. *Disturbance feedforward control for vibration isolation systems*. PhD thesis, Eindhoven University of Technology, 2018.

[9] M. A. Beijen, M. F. Heertjes, H. Butler, and M. Steinbuch. Disturbance feedforward control for active vibration isolation systems with internal isolator dynamics. *Journal of Sound and Vibration*, 436:220–235, 2018.

[10] S. Bingulac and R. Krtolica. On admissibility of pseudoobservability and pseudocontrollability indexes. *IEEE transactions on automatic control*, 32(10):920–922, 1987.

[11] C. Bohn and H. Unbehauen. Minmax and least squares multivariable transfer function curve fitting: Error criteria, algorithms and comparisons. In *Proceedings American Control Conference*, volume 5, pages 3189–3193. IEEE, 1998.

[12] R. Callafon. *Identification for control of complex motion systems*. PhD thesis, Delft University of Technology, 1998.

[13] D. Cressey and E. Callaway. Cryo-electron microscopy wins chemistry nobel. *Nature News*, 550(7675):167, 2017.

[14] R. A. De Callafon and P. M. Van den Hof. Suboptimal feedback control by a scheme of iterative identification and control design. *Mathematical modelling of systems*, 3(1):77–101, 1997.

[15] R. A. de Callafon and P. M. Van den Hof. Multivariable feedback relevant system identification of a wafer stepper system. *IEEE Transactions on Control Systems Technology*, 9(2):381–390, 2001.

[16] A. De Kraker and D. H. van Campen. *Mechanical vibrations*. Shaker-Verlag, 2001.

[17] M. de Mathelin and M. Bodson. Canonical vs pseudo-canonical forms for the structural and parametric identification of multivariable systems. In *Proceedings European Control Conference*, volume 2, pages 1282–1287, 1991.

[18] R. de Rozario. Identifying position-dependent mechanical systems: a physics-based LPV approach, with application to a wafer stage. Master's thesis, Eindhoven University of Technology, the Netherlands, 2015.

[19] S. G. Douma and P. M. Van den Hof. Relation between uncertainty structures in identification for robust control. volume 36, pages 33–38. Elsevier, 2003.

[20] J. M. Galvin, G. Ezzell, A. Eisbrauch, C. Yu, B. Butler, Y. Xiao, I. Rosen, J. Rosenman, M. Sharpe, L. Xing, et al. Implementing imrt in clinical practice: a joint document of the american society for therapeutic radiology and oncology and the american association of physicists in medicine. *International Journal of Radiation Oncology, Biology and Physics*, 58(5):1616–1634, 2004.

[21] M. Gevers and V. Wertz. Techniques for the selection of identifiable parametrizations for multivariable linear systems. *Control and Dynamic Systems*, 26:35, 2012.

[22] L. Giarre, M. Milanese, and M. Taragna. $\mathcal{H}_\infty$ identification and model quality evaluation. *IEEE Transactions on Automatic control*, 42(2):188–199, 1997.

[23] K. Glover and J. Willems. Parametrizations of linear dynamical systems: Canonical forms and identifiability. *IEEE Transactions on Automatic Control*, 19(6):640–646, 1974.

[24] L. Gonzalez-Macia, A. Morrin, M. R. Smyth, and A. J. Killard. Advanced printing and deposition methodologies for the fabrication of biosensors and biodevices. *Analyst*, 135(5):845–867, 2010.

[25] R. P. Guidorzi. Invariants and canonical forms for systems structural and parametric identification. *Automatica*, 17(1):117–133, 1981.

[26] F. Gustafsson and H. Hjalmarsson. Twenty-one ml estimators for model selection. *Automatica*, 31(10):1377–1392, 1995.

[27] M. Hazewinkel and R. E. Kalman. On invariants, canonical forms and moduli for linear, constant, finite dimensional, dynamical systems. In *Mathematical Systems Theory*, pages 48–60. Springer, 1976.

[28] A. Hendriks. Passieve demping in mechanische systemen. Master's thesis, Eindhoven University of Technology, the Netherlands, 2004.

[29] J. P. Hespanha. *Linear systems theory*. Princeton university press, 2018.

[30] D. W. Jorgenson, K. J. Stiroh, R. J. Gordon, and D. E. Sichel. Raising the speed limit: Us economic growth in the information age. *Brookings papers on economic activity*, 2000(1):125–235, 2000.

[31] T. Kailath. *Linear systems*, volume 156. Prentice-Hall Englewood Cliffs, 1980.

[32] H. K. Khalil. Nonlinear systems. *Upper Saddle River*, 2002.

[33] S. H. Kim, S.-H. Lee, and C. C. Chung. Phase shift calibration method in optical sinusoidal encoder signals applied to servo track writer. *IFAC-PapersOnLine*, 49(21):1–6, 2016.

[34] S. Konishi and G. Kitagawa. Generalised information criteria in model selection. *Biometrika*, 83(4):875–890, 1996.

[35] M. Kuijk. Auto calibration of incremental analog quadrature encoders. Master's thesis, Eindhoven University of Technology, the Netherlands, 2009.

[36] C. Mayda. Identification and mimo feedback control of nano-positioning flexible motion systems. Master's thesis, Eindhoven University of Technology, the Netherlands, 2016.

[37] D. C. McFarlane and K. Glover. *Robust controller design using normalized coprime factor plant descriptions*, volume 138. Springer, 1990.

[38] M. Milanese and M. Taragna. Optimality, approximation, and complexity in set membership $\mathcal{H}_\infty$-identification. *IEEE Transactions on Automatic Control*, 47(10):1682–1690, 2002.

[39] J. Mokyr. *The gifts of Athena: Historical origins of the knowledge economy*. Princeton University Press, 2002.

[40] G. E. Moore et al. Cramming more components onto integrated circuits, 1965.

[41] R. R. Nelson and E. S. Phelps. Investment in humans, technological diffusion, and economic growth. *The American economic review*, 56(1/2):69–75, 1966.

[42] T. Oomen and O. Bosgra. Robust-control-relevant coprime factor identification: A numerically reliable frequency domain approach. In *American Control Conference*, pages 625–631. IEEE, 2008.

[43] T. Oomen and O. Bosgra. System identification for achieving robust performance. *Automatica*, 48(9):1975–1987, 2012.

[44] T. Oomen, S. Quist, R. van Herpen, and O. Bosgra. Identification and visualization of robust-control-relevant model sets with application to an industrial wafer stage. In *IEEE Conference on Decision and Control*, pages 5530–5535. IEEE, 2010.

[45] T. Oomen, R. van der Maas, C. R. Rojas, and H. Hjalmarsson. Iterative data-driven norm estimation of multivariable systems with application to robust active vibration isolation. *IEEE Transactions on Control Systems Technology*, 22(6):2247–2260, 2014.

[46] T. Oomen, R. van Herpen, and O. Bosgra. Robust-control-relevant coprime factor identification with application to model validation of a wafer stage. volume 42, pages 1044–1049. Elsevier, 2009.

[47] T. Oomen, R. van Herpen, S. Quist, M. van de Wal, O. Bosgra, and M. Steinbuch. Connecting system identification and robust control for next-generation motion control of a wafer stage. *IEEE Transactions on Control Systems Technology*, 22(1):102–118, 2013.

[48] J. R. Rice. *The approximation of functions: linear theory*, volume 1. Addison-Wesley Reading, Mass., 1964.

[49] C. Sanathanan and J. Koerner. Transfer function synthesis as a ratio of two complex polynomials. *IEEE transactions on automatic control*, 8(1):56–58, 1963.

[50] R. S. Sanchez-Pena and M. Sznaier. *Robust systems theory and applications*. Wiley New York, 1998.

[51] R. J. Schrama. Accurate identification for control: The necessity of an iterative scheme. *IEEE Transactions on automatic control*, 37(7):991–994, 1992.

[52] G. Schwarz et al. Estimating the dimension of a model. *The annals of statistics*, 6(2):461–464, 1978.

[53] N. K. Sinha and G. P. Rao. *Identification of continuous-time systems: Methodology and computer implementation*, volume 7. Springer Science & Business Media, 2012.

[54] S. Skogestad and I. Postlethwaite. *Multivariable feedback control: analysis and design*, volume 2. Wiley New York, 2007.

[55] T. Soderstrom and P. Stoica. *System identification*. Prentice-Hall, Inc., 1988.

[56] P. Stoica and Y. Selen. Model-order selection: a review of information criterion rules. *IEEE Signal Processing Magazine*, 21(4):36–47, 2004.

[57] K. Tan, T. Lee, H. Dou, and S. Lim. Various developments in mechatronics in asia. *Mechatronics*, 8(7):777–791, 1998.

[58] T. van Bommel. Improving wafer stage motion performance through robust-control-relevant model set identification and multivariable control. Master's thesis, Eindhoven University of Technology, the Netherlands, 2010.

[59] T. van Bommel. Exploiting additional actuators and sensors for control of a nano-positioning system: a loop-shaping approach. Master's thesis, Eindhoven University of Technology, the Netherlands, 2017.

[60] M. van de Wal, G. van Baars, F. Sperling, and O. Bosgra. Multivariable μ feedback control design for high-precision wafer stage motion. *Control Engineering Practice*, 10(7):739–755, 2002.

[61] R. van Herpen, T. Oomen, and O. Bosgra. A robust-control-relevant perspective on model order selection. In *Proceedings American Control Conference*, pages 1224–1229. IEEE, 2011.

[62] J. Vayssettes, G. Mercère, and O. Prot. New developments for matrix fraction descriptions: A fully-parametrised approach. *Automatica*, 66:15–24, 2016.

[63] C. Verbaan. *Robust mass damper design for bandwidth increase of motion stages*. PhD thesis, Eindhoven University of Technology, the Netherlands, 2015.

[64] G. Vinnicombe. *Uncertainty and Feedback: $\mathcal{H}_\infty$ Loop-shaping and the ν-gap Metric.* World Scientific, 2001.

[65] R. Voorhoeve. *Identification for advanced motion control: numerically reliable algorithms for complex motion systems.* PhD thesis, Eindhoven University of Technology, 2018.

[66] R. Voorhoeve, R. de Rozario, and T. Oomen. Identification for motion control: Incorporating constraints and numerical considerations. In *Proceedings American Control Conference*, pages 6209–6214. IEEE, 2016.

[67] A. Whitfield. Asymptotic behaviour of transfer function synthesis methods. *International Journal of Control*, 45(3):1083–1092, 1987.

[68] K. Zhou, J. C. Doyle, K. Glover, et al. *Robust and optimal control*, volume 40. Prentice hall New Jersey, 1996.